



Systematic pharmacological analysis of agonistic and antagonistic fibroblast growth factor receptor 1 MAbs reveals a similar unique mode of action

Received for publication, August 19, 2022, and in revised form, November 11, 2022 Published, Papers in Press, November 19, 2022,

<https://doi.org/10.1016/j.jbc.2022.102729>

Jocelyn Chan^{1,‡}, Joyce Chan^{2,‡}, Lily Shao¹, Scott S. Stawicki³, Victoria C. Pham⁴, Rob W. Akita¹, Marc Hafner⁵, Lisa Crocker⁶, Kebing Yu⁴, James T. Koerber³, Gabriele Schaefer^{1,*}, and Laetitia Comps-Agrar^{2,*}

From the ¹Department of Molecular Oncology, Genentech Inc, South San Francisco, California, USA; ²Department of Biochemical and Cellular Pharmacology, Genentech Inc, South San Francisco, USA; ³Department of Antibody Engineering, ⁴Department of Microchemistry, Proteomics, Lipidomics and NGS, ⁵Department of Oncology Bioinformatics, and ⁶Department of Translational Oncology, Genentech Inc, South San Francisco, California, USA

Edited by Kirill Martemyanov

Fibroblast growth factor receptor 1 (FGFR1) is a receptor tyrosine kinase that plays a major role in developmental processes and metabolism. The dysregulation of FGFR1 through genetic aberrations leads to skeletal and metabolic diseases as well as cancer. For this reason, FGFR1 is a promising therapeutic target, yet a very challenging one due to potential on-target toxicity. More puzzling is that both agonistic and antagonistic FGFR1 antibodies are reported to exhibit similar toxicity profiles *in vivo*, namely weight loss. In this study, we aimed to assess and compare the mechanism of action of these molecules to better understand this apparent contradiction. By systematically comparing the binding of these antibodies and the activation or the inhibition of the major FGFR1 signaling events, we demonstrated that the molecules displayed similar properties and can behave either as an agonist or antagonist depending on the presence or the absence of the endogenous ligand. We further demonstrated that these findings translated in xenografts mice models. In addition, using time-resolved FRET and mass spectrometry analysis, we showed a functionally distinct FGFR1 active conformation in the presence of an antibody that preferentially activates the FGFR substrate 2 (FRS2)-dependent signaling pathway, demonstrating that modulating the geometry of a FGFR1 dimer can effectively change the signaling outputs and ultimately the activity of the molecule in preclinical studies. Altogether, our results highlighted how bivalent antibodies can exhibit both agonistic and antagonistic activities and have implications for targeting other receptor tyrosine kinases with antibodies.

Fibroblast growth factor (FGF) signaling is ubiquitous and regulates major homeostatic processes, such as developmental processes, metabolism, and phosphate homeostasis. Deregulation of FGF signaling can cause diseases through gain- or

loss-of-function mutations in FGF ligands or receptors (1, 2). Among these diseases are many skeletal syndromes, lacrimo-auriculo-dento-digital syndrome, and cancers. FGF receptor (FGFR) is therefore an attractive therapeutic target to treat a wide variety of pathologies. However, therapeutic targeting of FGFR may require either an agonist or antagonist depending on the indication, and a thorough understanding of the mechanism of action of the therapeutic molecule is critical.

In humans, four FGF receptors (FGFR1-4) exist and can be activated by 18 different FGFs (3). The FGFRs belong to the receptor tyrosine kinase (RTK) superfamily and consist of three extracellular immunoglobulin domains (D1-D3), a single-pass transmembrane (TM) domain, and a cytoplasmic tyrosine kinase domain (KD) (4). The D2-D3 fragment constitutes the FGF-binding domain (5), whereas D1 and an 8-residue acid box fragment between D1 and D2 play a role in receptor auto-inhibition (6). Alternative splicing of exons encoding the C-terminal part of D3 of FGFR1-3 results in the generation of b and c isoforms that determine FGF-binding specificities (7). The specificity of canonical FGF:FGFR binding is also determined by association with cofactor heparin/heparan sulfate proteoglycans (HSPGs), whereas endocrine FGFs evolved to reduce affinity towards HSPG and rely on binding to Klotho coreceptors instead (8). Canonical FGFs can act in an autocrine or paracrine manner and play a critical role during embryogenesis and organogenesis to promote growth, differentiation, and tissue patterning. In adult tissues, these FGFs regulate a wide variety of physiological processes including but not limited to cell fate, developmental processes, angiogenesis, and immunity (2). In addition to canonical FGFs, there are three human endocrine FGFs (FGF19, FGF21, and FGF23) that carry out diverse functions such as regulating bile acid, carbohydrate and lipid metabolism, as well as phosphate homeostasis (9–11).

Binding of canonical FGF to FGFR results in the formation of a functional unit consisting of two 1:1:1 FGF–FGFR–HSPG complexes juxtaposed in a symmetrical dimer (12). In this configuration, each ligand simultaneously contacts both receptors, and the receptor ectodomain interacts through a four

[‡] These authors contributed equally to this work.

* For correspondence: Laetitia Comps-Agrar, compsagl@gene.com; Gabriele Schaefer, schaefer.gabriele@gene.com.

Present address for Kebing Yu: Fuhong Therapeutics; Shanghai 310,000, China.

Elucidation of the mode of action of FGFR1 monoclonal antibodies

amino acid residue patch in D2. Stabilization of the FGFR dimer results in a conformational change in the TM domain that brings the intracellular KDs into proximity and into a favorable orientation towards each other, allowing transphosphorylation and activation of the KDs to occur (13, 14). In turn, the KDs activate intracellular substrates through a cascade of phosphorylation events. Among them, two major substrates determine the fate of the two main signaling pathways activated by FGFRs: namely the adaptor protein FGFR substrate 2 α (FRS2 α) and phospholipase C γ 1 (PLC γ 1). FRS2 α phosphorylation leads to activation of the RAS/mitogen-activated protein kinase (MAPK) pathway and the PI3K/protein kinase B (AKT) pathway, whereas PLC γ 1 is necessary and sufficient to trigger the release of intracellular calcium stores and activation of PKC (8, 15).

Receptor agonism may provide a therapeutic strategy for certain indications. For example, FGF21, an endocrine FGF that binds FGFR1c/Klotho-b complex, gained a lot of attention for its potential antiobesity and antidiabetic properties after several preclinical studies demonstrated its ability to improve insulin sensitivity, hepatosteatosis, and increase weight loss (9, 16). Several FGF21 mimetics are now actively being pursued in the clinic for the treatment of type 2 diabetes and nonalcoholic steatohepatitis. Engineering these molecules to make them suitable for therapeutic use has been a considerable challenge for pharmaceutical companies for diverse reasons including short half-life, aggregation and proteolysis of FGF21 analogs, toxicity of FGFR1 antibodies (Abs), etc. (17). As an example, R1MAb1 and R1MAb2 are FGFR1 phage-derived MABs that were selected for their agonistic activity and FGF21-like antidiabetic and lipid-lowering properties in preclinical studies (18). Although efficient at promoting weight loss in obese mice, the use of R1MABs resulted in the elevation of serum FGF23 and hypophosphatemia, which ultimately led to the discontinuation of the clinical use of these Abs (19).

Conversely, receptor antagonism is desired for other indications, such as cancer. Amplification of chromosomal region 8p11-12 bearing FGFR1 is observed in approximately 6% of all lung cancer patients and 10% of breast cancer patients, predominantly in cases of estrogen receptor (ER) positive cancer. The resulting elevated FGFR1 expression correlates with poor prognosis (20). To date, most of the molecules in the clinic targeting FGFR for cancer indications are small molecule inhibitors that target an ATP-binding pocket well-conserved among FGFRs and FGFR-related RTKs (21). When dealing with molecules presenting low specificity towards a given target, one could expect a wide range of off-target toxicity effects in addition to the expected on-target toxicity. Such on-target toxicity effects include hyperphosphatemia as reported for a selective FGFR1-3 inhibitor (AZD4547) following a dose escalation in a phase 1 clinical study (22, 23).

As an alternative, Abs could provide a highly selective inhibitor for a specific FGFR isoform. While we and others were successful generating such molecules (21, 24, 25), this approach also comes with its own challenges. Antagonistic Abs can function by interfering with ligand binding and/or by

preventing receptor dimerization. However, the bivalent nature of immunoglobulin G (IgG) may in fact promote dimerization of receptors rather than prevent their interaction, resulting in receptor activation in the absence of endogenous ligand. Several preclinical studies report that antagonistic FGFR1 MABs induce weight loss, mimicking the phenotype observed with agonistic FGFR1 MABs (26, 27). This finding is in direct contrast to the preclinical and clinical data obtained with small molecule inhibitors of FGFR that do not show any weight loss but report the expected hyperphosphatemia.

In this study, we set out to reconcile this reported functional difference between Abs by elucidating the modes of action of two agonistic FGFR1 MABs (R1MAb) and an antagonistic FGFR1 MAB (IMC-H7 MAB). Here, we demonstrated that both R1MAb and IMC-H7 MAB display similar properties and can behave as an agonist or antagonist depending on the context. In addition, we described a functionally distinct FGFR1 active conformation in the presence of an antibody that preferentially activates the FRS2-dependent signaling pathway, demonstrating that modulating the geometry of a FGFR1 dimer can effectively change its signaling output.

Results

FGFR1 R1MAb1, R1MAb2, and IMC-H7 competed with FGF ligand binding

To begin to mechanistically understand the conflicting agonist/antagonist activities for three FGFR1 Abs (R1MAb1, R1MAb2 (18), and IMC-H7 MAB (26)), we sought to structurally characterize how they interacted with FGFR1. Overlay of the epitope of R1MAb1/2 that was identified using peptide ELISAs (18) onto the structure of FGFR1:FGF2 complex (PDB 1CVS) (5) showed that the epitope of R1MAb1/2 only partially overlapped with the FGF-binding site and more prominently overlapped with the presumed dimerization interface of FGFR1, suggesting that the MABs may not be direct ligand blockers (5, 28) (Fig. 1A). We then performed bio-layer interferometry (BLI)-based epitope binning and demonstrated that R1MAb1, R1MAb2, and IMC-H7 bound to overlapping epitopes (Figs. 1B and S1). In order to determine whether the binding of these Abs could prevent the binding of the natural ligand, we performed competitive binding experiments. COS7 cells transiently expressing FGFR1c were incubated with radiolabeled Iodine-125 FGF2 and increasing concentrations of nonlabeled FGFR1 Abs. We observed binding competition curves for R1MAb1, R1MAb2, and IMC-H7 MAB with a half-maximal inhibitory concentration (IC₅₀) of 6.6 \pm 3.7, 4.5 \pm 2.7, and 1.2 \pm 0.4 nM, respectively (Fig. 1C), demonstrating that although the MABs did not share the same binding site as FGF (Figs. 1, A, B and S1), they still potently prevented ligand binding most likely through steric hindrance and/or conformational changes in FGFR1c.

FGFR1 MABs and antigen-binding fragments inhibited FGFR1 signaling pathways activated by FGF

To understand the functional consequences of blocking FGF with FGFR1 Abs, we assessed key events in the FGFR1

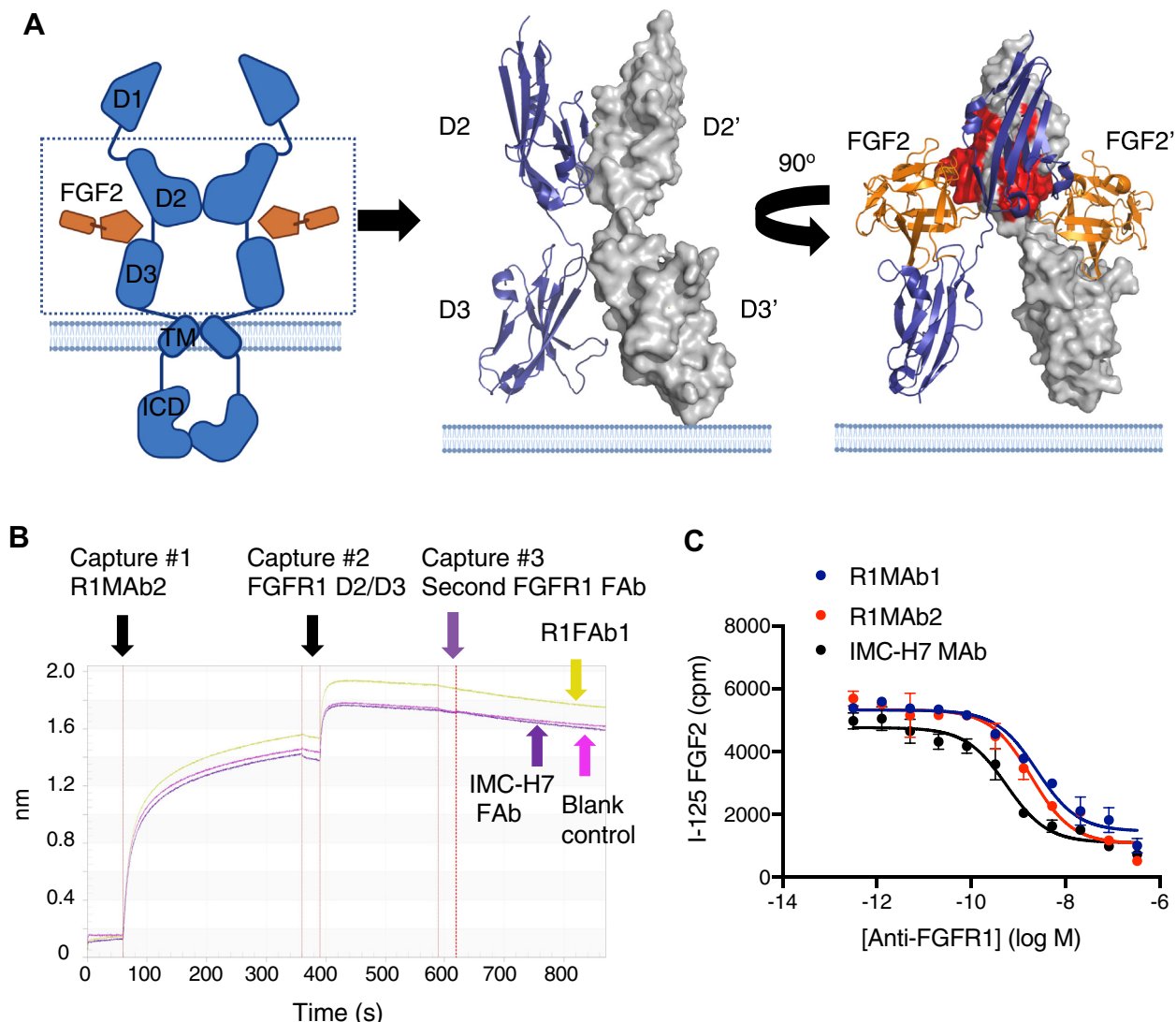


Figure 1. R1 and IMC-H7 MABs binding properties. *A*, overview of FGFR1 homodimer structure and relevant epitopes. The extracellular domain of FGFR1 contains three Ig domains (D1-D3). An existing crystal structure of the D2D3 domains of FGFR1 bound to FGF2 (PDB 1CVS) provides a more detailed view of the binding sites of FGF2 to FGFR1 and homodimerization interface of FGFR1 mediated through the D2 domains. One copy of FGFR1 is shown in *dark blue ribbons* and the other copy is shown as a *gray surface*. The two FGF2 proteins are colored in *orange*. The epitope of R1MAB1/2 (*red*) as determined by peptide ELISAs is colored in *red* and overlaps predominantly with the FGFR1 homodimerization interface (18). *B*, bio-layer interferometry (BLI)-based epitope binning demonstrates that R1MAB1, R1MAB2, and IMC-H7 bind to overlapping epitopes. R1MAB2 was captured on the surface and saturated with FGFR1 protein. R1FAB1 or IMC-H7 FAb were added. Neither the R1FAB1 or IMC-H7 FAb could bind to FGFR1 in the presence of R1MAB2. *C*, binding inhibition curves of anti-FGFR1 R1MAB1 (*blue circle*), R1MAB2 (*red circle*), and IMC-H7 MAb (*black circle*) in the presence of Iodine-125 FGF2 on COS7 cells expressing FGFR1c. Data are representative of two independent experiments performed in triplicates. Data are means \pm S.D. FGFR1, Fibroblast growth factor receptor 1.

signaling pathways: phosphorylation of FRS2 and ETS domain-containing protein Elk-1 (Elk1), a nuclear target for the MAPK signaling pathway, and recruitment of PLC γ 1 (Fig. 2A). We first tested increasing concentrations of the Abs in the presence of a fixed concentration of FGF2 and monitored the phosphorylation of the adaptor molecule FRS2 in COS7 cells transiently expressing FGFR1c. We observed partial blocking activities for all six molecules (Fig. 2B). We then assessed the FGFR1 MABs and corresponding antigen-binding fragments (FABs) in a β -galactosidase (GAL)-Elk1 luciferase reporter assay to monitor the MAPK pathway downstream of FRS2 phosphorylation. Our results showed that all three MABs and the corresponding FABs effectively blocked FGF2-

dependent luciferase activity (Fig. 2C). IMC-H7 MAB was the most potent blocking antibody with an IC₅₀ of 0.004 μ M.

In addition, we assessed PLC γ 1 recruitment, another major intracellular signaling pathway activated by FGFR1 activation. Using a β -GAL fragments complementation assay, we demonstrated that the FGFR1 Abs prevented the recruitment of PLC γ 1 to the receptor in the presence of FGF2, again supporting the antagonistic activity of the Abs to inhibit FGF2-mediated activation of FGFR1 (Fig. 2D).

To verify whether the antagonistic nature of the Abs could be recapitulated in a cell line with amplified FGFR1 level, but devoid of other FGFR family members, we treated the breast cancer cell line CAL-120 with FGF1 and increasing amounts of

Elucidation of the mode of action of FGFR1 monoclonal antibodies

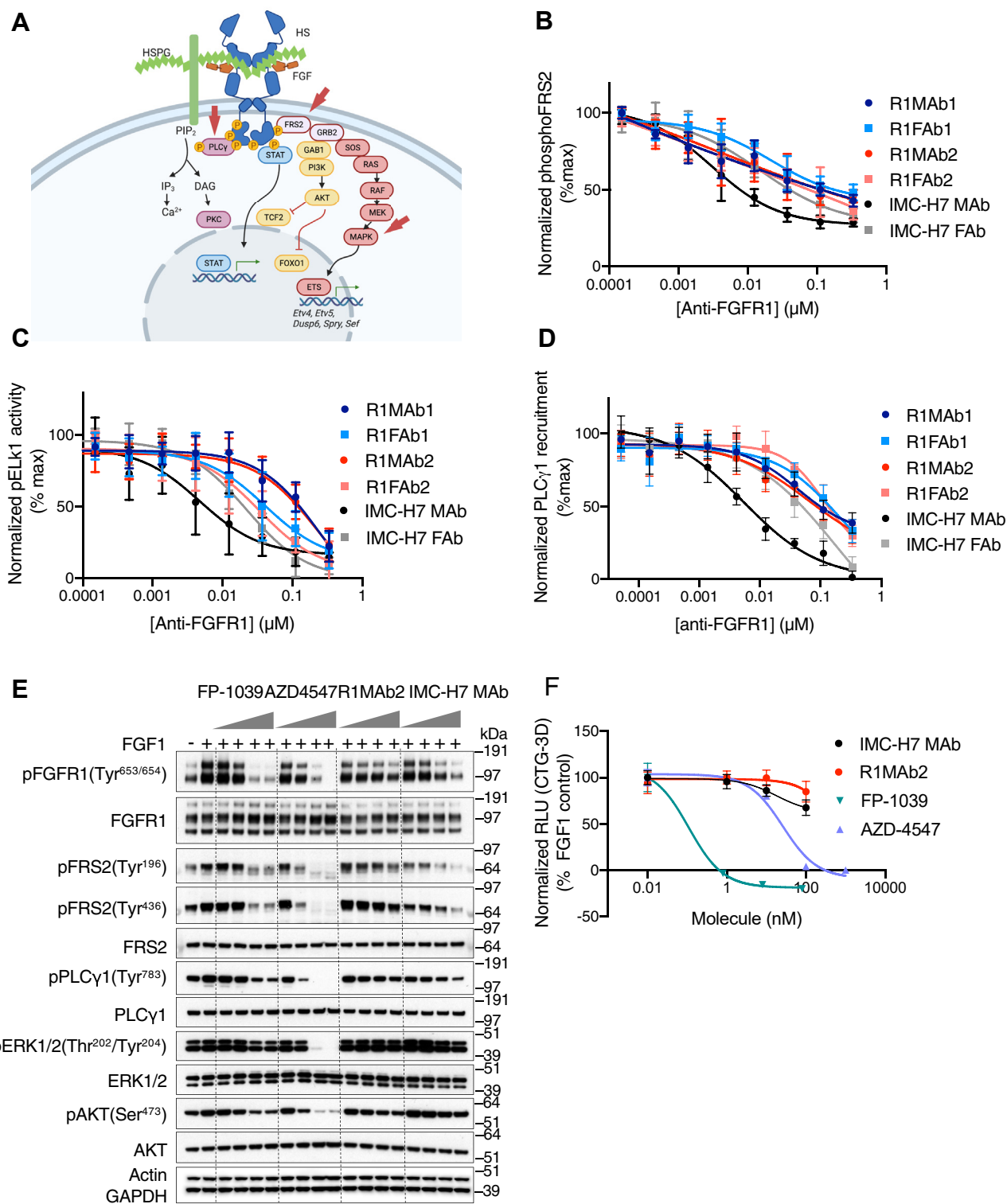


Figure 2. Impact of R1 and IMC-H7 MAbs and FAb on FGFR1-dependent signaling in the presence of FGF1 or FGF2. *A*, schematic representation of FGFR1 signaling pathways activated in response to FGF1/2 binding. Measurement of *(B)* FRS2 phosphorylation in COS7 cells, *(C)* Elk1 activity in COS7 cells, and *(D)* PLC γ 1 recruitment in U2OS cells expressing FGFR1c and incubated in the presence of a constant amount of FGF2 and increasing amounts of R1 and IMC-H7 MAbs or FAb. For *(B–D)*, data are normalized to the maximum signal obtained in the absence of Abs. Data are means \pm S.D. of at least three independent experiments performed in triplicate. *E*, immunoblots performed on lysates prepared from CAL-120 cells incubated in the presence of 0.3 nM FGF1 and 0.08 to 80 nM of FP-1039, 1 to 1000 nM of AZD4547, or 0.1 to 100 nM of R1MAb2 or IMC-H7 MAb. Immunoblots are representative of three independent experiments. The quantitation data from these three independent experiments are shown in Fig. S2. *F*, CAL-120 cells 7-days proliferation assay in the absence or presence of FGF1 (0.3 nM) and R1MAb2, IMC-H7 MAb, FGF ligand trap (FP-1039), or AZD4547. Data are normalized as follows: 100% = 0.3 nM FGF1 and 0% = no FGF1. Data are means \pm S.D. and are representative of three independent experiments. FGF, fibroblast growth factor; FGFR1, FGF receptor 1.

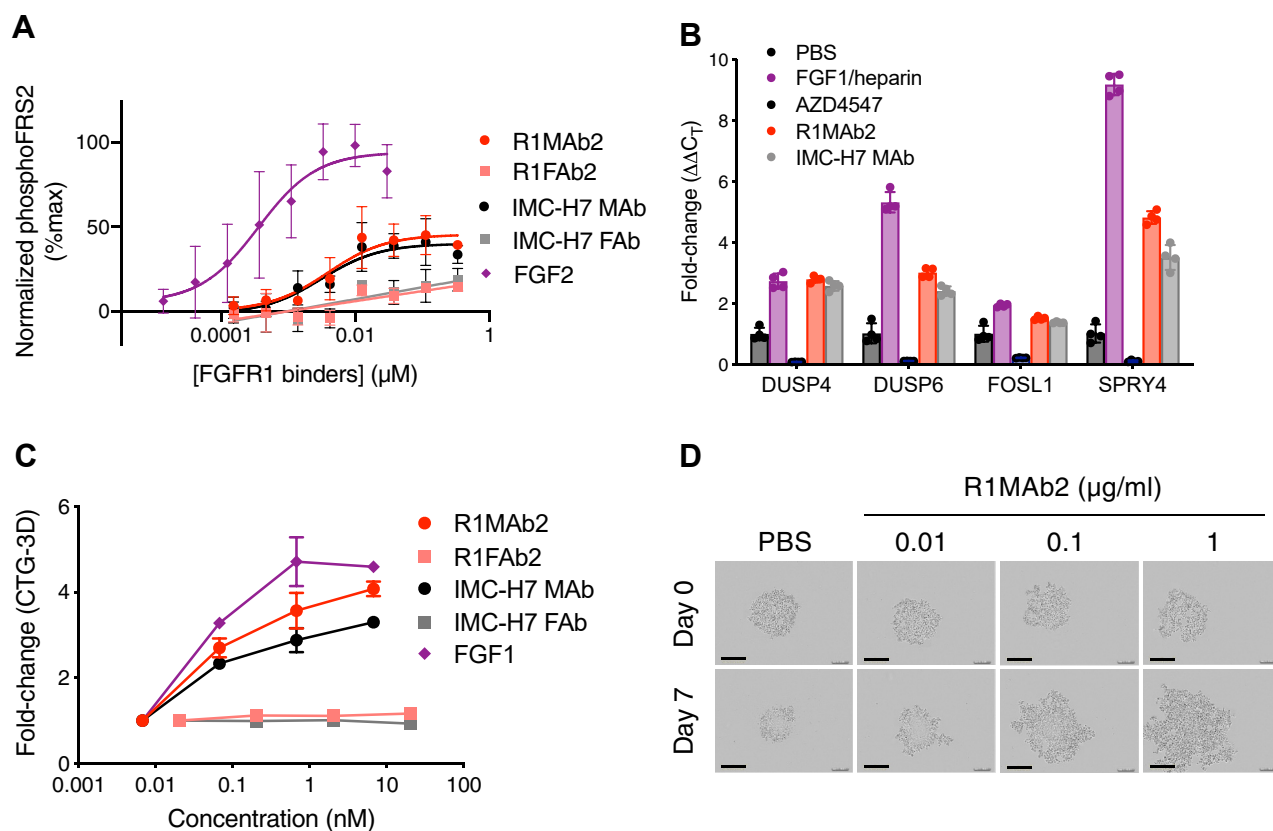


Figure 3. Impact of R1 and IMC-H7 MABs and FABs on FGFR1-dependent signaling in the absence of FGF ligands. *A*, measurement of FRS2 phosphorylation in COS7 cells expressing FGFR1c and incubated in the presence of increasing amounts of R1 and IMC-H7 MABs, FABs, or FGF2. Data are normalized to the maximum signal obtained with FGF2. Data are means \pm S.D. of at least three independent experiments performed in triplicate. *B*, MAPK target gene transcript levels in CAL-120 cells upon treatment with R1MAb2 (1 $\mu\text{g/ml}$), IMC-H7 MAb (1 $\mu\text{g/ml}$), or FGF small molecule inhibitor AZD4547 (0.2 μM) for 8 h. *C*, 7-days proliferation assay using CAL-120 cells treated with R1MAb2, R1FAb2, IMC-H7 MAb, IMC-H7 Fab, or FGF1 at indicated concentrations. *D*, representative images of cells treated with increasing amounts of R1MAb2 at day 0 and day 7 posttreatment. The scale bar represents 300 μm . *B-D*, data are means \pm S.D. and representative of three independent experiments, performed in triplicates. FGF, fibroblast growth factor; FGFR1, FGFR1; MAPK, mitogen-activated protein kinase.

R1MAb2, IMC-H7 MAb, AZD4547, a small molecule FGFR kinase inhibitor, or FP-1039, a FGFR1c extracellular domain fused with the Fc region of IgG1 (29). Phosphorylation of key proteins involved in FGFR1 downstream signaling was assessed with Western blot analysis. Consistent with our previous results, we observed decreased phosphorylation of FGFR1, FRS2, PLC γ 1, AKT, with both R1MAb2 and IMC-H7 MAb (Figs. 2E and S2). The FGFR1-dependent signaling pathway activated by FGF1 was, however, inhibited to a larger extent in the presence of AZD4547 and FP-1039 (Figs. 2E and S2). These observations were confirmed for R1MAb2 using the breast cancer cell line MDA-MB-134 that also overexpresses FGFR1 (Fig. S3).

Taken together, our data suggested that FGFR1 R1MAb1, R1MAb2, and IMC-H7 MABs and their respective FABs inhibited ligand-dependent activation of FGFR1. This was in agreement with the previously reported antagonistic activity of IMC-H7 MAB in the presence of ligand (26) and revealed the antagonistic activity of R1MAb1 and R1MAb2 under these conditions.

We next determined if the FGFR1 Abs were able to inhibit ligand-induced proliferation of CAL-120 cells in a 3D proliferation assay. CAL-120 cells were incubated with increasing

concentrations of R1MAb2, IMC-H7 MAb, AZD4547, or FP-1039 for 7 days. R1MAb2 or IMC-H7 MAb only minimally decreased cell growth, whereas AZD4547 and FP-1039, both known to decrease FGFR-dependent cell growth (22, 29), had a profound, dose-dependent effect on cell proliferation (Fig. 2F). These results suggested that the antagonistic activity of the FGFR1 MABs was not potent enough to cause an anti-proliferative effect.

FGFR1 MABs were partial FGFR1 agonists

Given the previously described agonistic activity of R1MAb2 (18) and the similar behavior of R1MAb2 and IMC-H7 MAB in our assays, we hypothesized that both Abs may display some degree of agonistic activity in the absence of ligand. To address this question, we assessed the phosphorylation of FRS2 in FGFR1c-expressing COS7 cells in the presence of increasing amounts of bivalent MABs or monovalent FABs. In this particular setting, no FGF was added to the cells. R1MAb1 and R1MAb2 exhibited almost identical binding and functional properties; therefore, we focused only on R1MAb2 for the next series of experiments. Both R1MAb2 and IMC-H7 MAB induced FRS2 phosphorylation to a similar extent, although

Elucidation of the mode of action of FGFR1 monoclonal antibodies

significantly less than that caused by FGF2 (% maximum activation of 45.5, 40.1, and 100% for R1MAb2, IMC-H7 MAb, and FGF2, respectively) (Fig. 3A). In contrast, the corresponding Fab versions failed to yield FRS2 phosphorylation, suggesting that the bivalent IgG may induce receptor dimerization and subsequent activation of FGFR1c.

Similar results were obtained in the GAL-Elk1 luciferase reporter assay, where R1MAb2 reached 13.9% maximum activation, while the Fab version was inactive (Fig. S4). IMC-H7 MAb had very minimal activity. Combined, these results suggested that these two MAbs exhibited different degrees of agonistic activity with IMC-H7 MAb being less potent and only able to initiate proximal signaling events, such as phosphorylation of FRS2 (pFRS2).

We also confirmed agonistic activity of the MAbs in the FGFR1-amplified CAL-120 cell line. Activation of FGFR1 resulted in a strong activation of the RAS-MAPK pathway *via* FRS2 phosphorylation (15). Treatment with FGF1, R1MAb2, or IMC-H7 MAb increased transcript levels of multiple MAPK target genes including dual specificity phosphatase (*DUSP4*), *DUSP6*, Fos-related antigen 1 (*FOSL1*), and Sprouty RTK signaling antagonist 4 (*SPRY4*) (Fig. 3B). Consistent with our reporter assay data, ligand stimulation induced the strongest agonistic response (Fig. 3B).

We next sought to explore the effect of the MAbs on CAL-120 proliferation. In the presence of increasing concentrations of R1MAb2 and IMC-H7 MAb, we observed a 3- to 4-fold enhancement of cell growth, similar to that of FGF1 (Fig. 3C) and obtained representative spheroid images with R1MAb2 (Fig. 3D). Consistent with our signaling experiments (Figs. 3A and S4), monovalent binding of R1MAb2 Fab and IMC-H7 Fab did not induce cell proliferation. Taken together, our data indicated that the three FGFR1 Abs have agonistic properties and that bivalency is required to activate the FGFR1 signaling pathway.

FGFR1 MAbs did not activate PLC γ -dependent signaling pathway

Since the bivalent R1MAb2 and IMC-H7 MAb (but not their respective Fabs) activated FGFR1, we hypothesized that the MAbs dimerize two FGFR1 monomers, which leads to subsequent receptor activation. To assess the impact of FGF versus the MAbs on FGFR1 complex formation, we labeled cell-surface N-terminal SNAP-tagged FGFR1 with time-resolved FRET (TR-FRET) compatible fluorophores and monitored the TR-FRET signal similar to what we previously described (30). In the presence of FGF2, we observed a 2.8-fold increase in the TR-FRET signal indicative of the formation of fully active FGFR1c dimers (Fig. 4A). R1MAb2 and IMC-H7 MAb also induced an increase of the TR-FRET signal but to a lesser extent (1.7- and 2-fold increases for R1MAb2 and IMC-H7 MAb, respectively). Their respective Fabs did not modulate the TR-FRET signal, suggesting that bivalency is necessary for dimerization of the receptor. The significant difference in TR-FRET signal between FGF2 and the MAbs

suggested a different geometry and/or stability of the FGFR1c dimers and likely reflected the partial agonist activity of FGFR1 Abs.

To investigate the functional consequences resulting from different FGFR1 complex organizations, we compared downstream signaling changes in CAL-120 cells in the presence of R1MAb2, IMC-H7 MAb, or FGF1. Western blot analysis revealed an increase of phosphorylation of FGFR1 (Tyr^{653/654}), FRS2, ERK1/2, and AKT in all treatment conditions, although the phosphorylation induced by R1MAb2 and IMC-H7 MAb was significantly less than that caused by the ligand stimulation, consistent with what we previously described (Figs. 4B and S5). We did not observe phosphorylation of PLC γ 1 (Figs. 4B and S5) nor did we observe recruitment of PLC γ 1 to FGFR1 upon R1MAb2 or IMC-H7 MAb treatment (Fig. 4C). The PLC γ 1-docking site Tyr⁷⁶⁶ on FGFR1 (15, 31) was not phosphorylated in the presence of R1MAb2 and IMC-H7 MAb, explaining the absence of PLC γ 1 recruitment (Fig. 4C). Collectively, these results indicated that these FGFR1 MAbs have a unique mechanism of action compared to the natural ligand.

To identify additional signaling differences between R1MAb2 and FGF1 stimulation, we assessed phosphorylation of key signaling proteins in CAL-120 cells in both treatment conditions using a human phospho-kinase array kit. We noticed one major signaling alteration between the two groups: the phosphorylation of cAMP response element-binding protein (CREB) appeared significantly reduced in the R1MAb2-treated samples (Fig. 4D). To determine whether CREB phosphorylation induced by FGFR1 pathway activation was mediated through PLC γ 1, we compared FGF1- or R1MAb2-induced downstream signaling in parental or PLC γ 1 knock-down CAL-120 cells. FGF1-induced phosphorylation of CREB was significantly reduced in the absence of PLC γ 1. Furthermore, we did not observe CREB phosphorylation in parental and PLC γ 1 knockdown CAL-120 cells upon R1MAb2 treatment, consistent with the inability of R1MAb2 to trigger PLC γ 1 recruitment and activation (Fig. 4E).

Finally, we measured calcium release upon treatment with FGFR1 MAbs or FGF2 in FGFR1c-expressing cells as this is reported to be downstream of PLC γ 1 signaling pathway activation (8, 15). As expected, FGF2 induced a dose-dependent increase in calcium release (Fig. 4F). However, R1MAb2 and IMC-H7 MAb failed to induce calcium release, confirming the inability of the FGFR1 Abs to activate the PLC γ 1-dependent signaling pathway. In summary, our data showed that FGFR1 MAbs selectively activated FGFR1 signaling through FRS2 phosphorylation but failed to recruit PLC γ 1 and impact subsequent signaling events, unlike the natural ligands FGF1 and FGF2.

Unique phosphorylation signature of FGFR1 upon stimulation with FGFR1 MAb explained the absence of PLC γ 1 recruitment

Western blot analysis as well as functional assays showed that FGFR1 MAbs activated FRS2- but not PLC γ 1-dependent

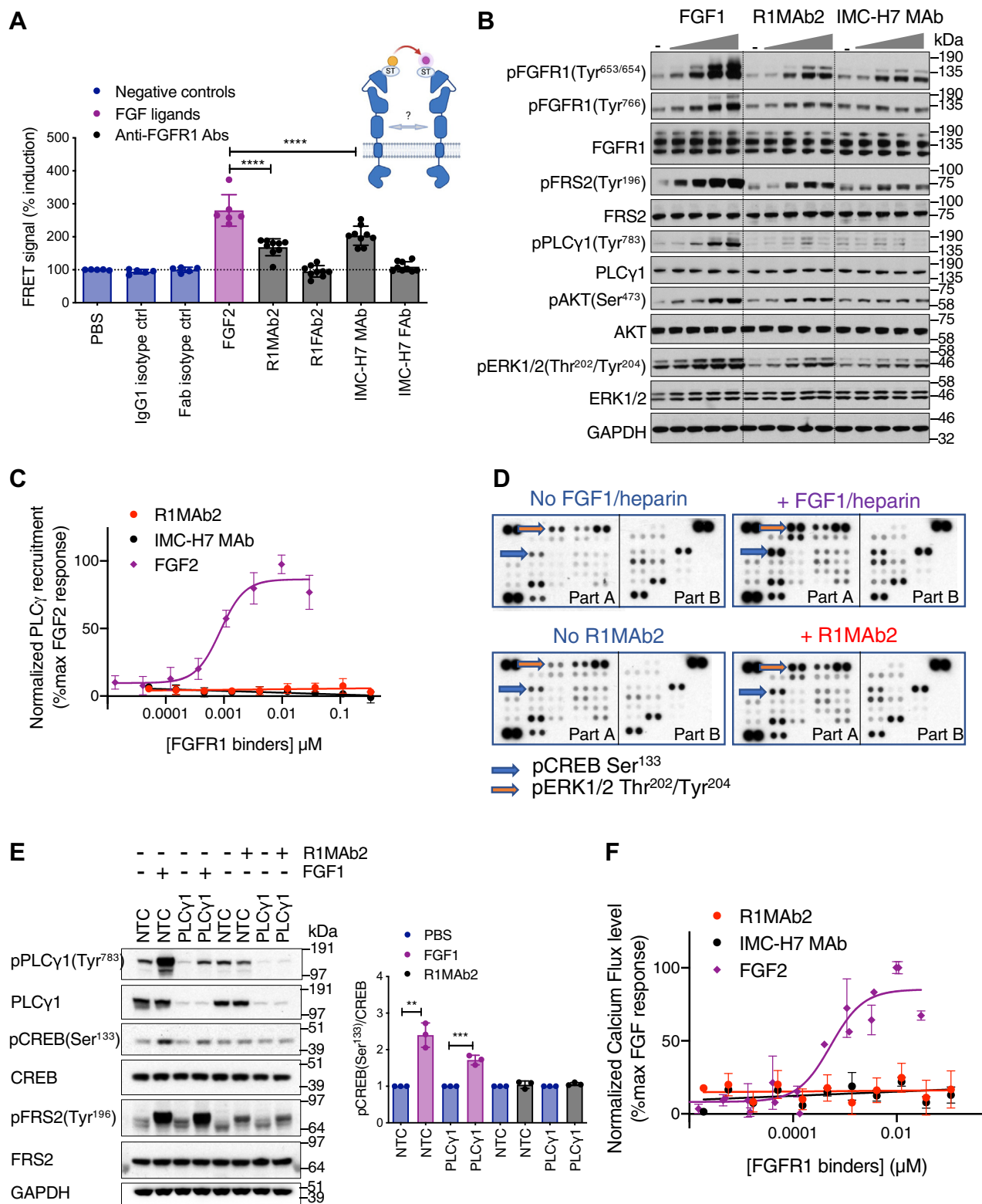


Figure 4. Assessment of differences in FGFR1 signaling pathways triggered by R1Mab2 or IMC-H7 MAb versus FGF ligands. A, cell-surface SNAP-tagged FGFR1c interaction determined using TR-FRET in the presence of buffer or isotype controls (blue histograms), FGF2 (purple histogram), or R1Mab2, FAB2, IMC-H7 MAb, and Fab (black histograms). Results are normalized to the TR-FRET signal obtained in the absence of stimulation. B, Western blot analysis performed using lysates prepared from FGFR1-amplified CAL-120 cells incubated with a concentration range of FGF1 starting at 1 nM or a concentration range of R1Mab2 or IMC-H7 MAb starting at 10 nM. Immunoblots are representative of three independent experiments. The quantitation data from these three independent experiments are shown in Fig. S5. C, PLCγ1 recruitment measured in U2OS cells expressing ProLink tagged FGFR1c and an Enzyme Acceptor tagged SH2 domain in the presence of increasing amounts of R1Mab2, IMC-H7 MAb, or FGF2. D, phosphorylation status of cancer-related kinases assessed using phospho-kinase arrays in CAL-120 cells treated with FGF1/heparin or R1Mab2. Array Part A contains 29 Abs printed in duplicate, and array Part B contains 16 Abs printed in duplicate. All arrays were processed at the same time. E, immunoblots and quantitation data of FGFR1 downstream signaling molecules performed with lysates from CAL-120 cells transfected with either a nontargeting control (NTC) or PLCY1 siRNA and treated with FGF1 or

Elucidation of the mode of action of FGFR1 monoclonal antibodies

signaling pathways, which implies that treatment with the agonistic Abs or treatment with FGFR ligands may result in distinct phosphorylation events. To comprehensively identify receptor or signaling intermediates activated downstream of FGFR1, we performed global tyrosine phosphoproteomic analysis and compared FGF1 or R1MAb2 treated to control treated CAL-120 cells (Figs. 5A, S6, A and B). Overall, there were about 6000 total peptide spectral matches (PSMs) containing tyrosine phosphorylated species that matched about 950 proteins with phospho-tyrosine (pTyr) from which 5700 total PSMs were quantifiable (isolation specificity ≥ 0.5). The peptide coverage of main proteins of interest assessed was summarized (Fig. S7). The total number of pTyr sites detected was greater upon FGF1 versus R1MAb2 treatment (Figs. 5B and S6C). The level of all the major unique FGFR1 pTyr sites increased upon addition of FGF1 (Fig. 5, C and D), but only pTyr⁶⁵³, a phosphorylation site that results in 50- to 100-fold increased kinase activity (15), was more abundant in both conditions (Fig. 5C). Consistent with our previous results indicating antibody-mediated receptor activation through FRS2, the proportion of most pTyr sites on FRS2 showed enhanced phosphorylation in both treatments except for pTyr¹⁵⁰ which was only phosphorylated in the presence of FGF1. Downstream of FRS2, pTyr¹⁸⁵ on ERK1/2 and pTyr⁶⁵⁹ growth factor receptor-bound protein 2-associated protein 1 (Gab1) were induced by both treatments.

As expected, PLC γ 1 pTyr sites were only phosphorylated upon FGF1 incubation (Fig. 5D). Overall, we did not identify any pTyr that were uniquely phosphorylated on the receptor or on downstream effector proteins in the presence of FGFR1 MAbs.

Altogether, our mass spectrometry analysis confirmed our previous functional data and revealed that treatment with R1MAb2 induced a distinct FGFR1 phosphorylation profile, in which only residue pTyr⁶⁵³ was phosphorylated leading to the activation of the FRS2-dependent signaling pathway.

R1MAb2 and IMC-H7 agonistic effect is predominant in vivo

In vitro studies demonstrated that both FGFR1 MAbs can act as agonist or antagonist depending on the presence or absence of the natural ligand. In order to determine which pharmacological effect is dominant *in vivo*, we sought to investigate the effect of R1MAb2, IMC-H7 MAb, or the well-validated small molecule inhibitor AZD4547 on the tumor growth of CAL-120 breast xenografts in C.B-17 SCID mice. We previously verified that CAL-120 cells relied on FGFR1 expression for proliferation (Fig. S8A). In this model, antagonistic activity would lead to CAL-120 tumor regression, while agonistic activity would not attenuate tumor growth and would cause mice body weight loss. As expected from an FGFR1 antagonist, AZD4547 administration did not result in body weight loss but led to a significant tumor regression

(Figs. 6, S8, B and C). In contrast, a single injection of R1MAb2 or IMC-H7 MAb resulted in a substantial body weight loss (Fig. 6). The amplitude of the weight loss was more significant for the R1MAb2 group and resulted in the termination of all the mice on or before day 5. IMC-H7 MAb that displayed a lower agonistic activity *in vitro* induced a less substantial body weight loss (-10.2% at day 3) and the mice remained in the study (Fig. 6). However, to preserve the welfare of the mice, no additional doses of IMC-H7 MAb were administered; therefore, the potential effect on tumor growth could not be assessed. To conclude, this study demonstrated that the agonistic activity observed for both FGFR1 MAbs is predominant *in vivo* and is responsible for the toxicity that manifested as a substantial weight loss. Similar to our *in vitro* results, the agonist effect of R1MAb2 was stronger than that of IMC-H7 MAb *in vivo*.

In summary, our study highlighted a distinct mechanism of action of FGFR1 MAbs where in the absence of FGF ligands, the Abs acted as partial agonists on the FRS2-dependent signaling pathway. In this configuration, PLC γ 1 was not recruited (Fig. 7). Likely, the distance between the FGFR1 extracellular domains (ECDs) was increased in the presence of the Abs as compared to natural ligands, resulting in a suboptimal transphosphorylation of the KDs under this condition. We do not have any data supporting a specific arrangement of the TMs or the KDs and their position in the model is speculative. In the presence of FGF ligands, R1MAb2 and IMC-H7 MAb acted as competitive antagonists by sterically hindering FGF binding and, therefore, decreasing the signaling outcomes from FRS2- and PLC γ 1-dependent signaling pathways (Fig. 7).

Discussion

The RTK family is an important target for therapeutics across multiple indications. Among the therapeutic options, mAbs are yielding transformative results in the clinic. Bivalent Abs can naturally induce RTK dimerization and activation, thus generating and selecting Abs capable of antagonizing receptor signaling can be challenging. However, we can refer to successful examples such as trastuzumab and pertuzumab that are approved for the treatment of human epidermal growth factor receptor 2 (HER-2) positive breast cancer (32–35) or the epidermal growth factor receptor (EGFR) targeting Abs cetuximab and panitumumab, both indicated for the treatment of colorectal and head and neck cancers (36). In the FGFR field, a few antagonistic Abs show promising results in preclinical studies (37) and in clinical development: bemarituzumab for the treatment of gastric cancers harboring FGFR2b overexpression and vofatamab (B-701) indicated for urothelial carcinomas harboring FGFR3 alterations (21, 24). The common denominator between all these molecules is a unique mechanism of action that allows for the inhibition of the downstream signaling pathway and subsequent cell

R1MAb2 48 h posttransfection. The quantitation data are means \pm S.D. of three independent experiments. Student's *t*-tests for 2 comparisons: **p* < 0.05. *F*, calcium release signal measured upon stimulation of FGFR1c-expressing HEK293 cells with increasing amounts of R1MAb2, IMC-H7 MAb, or FGF2. For (C and F), data are normalized to the maximum signal obtained with FGF2. For (A, C, and F) data are means \pm S.D. of at least three independent experiments performed in triplicate. One-way ANOVA with Tukey's multiple comparison test: *****p* < 0.0001. FGF, fibroblast growth factor; FGFR1, FGF receptor 1; TR-FRET, time-resolved FRET.

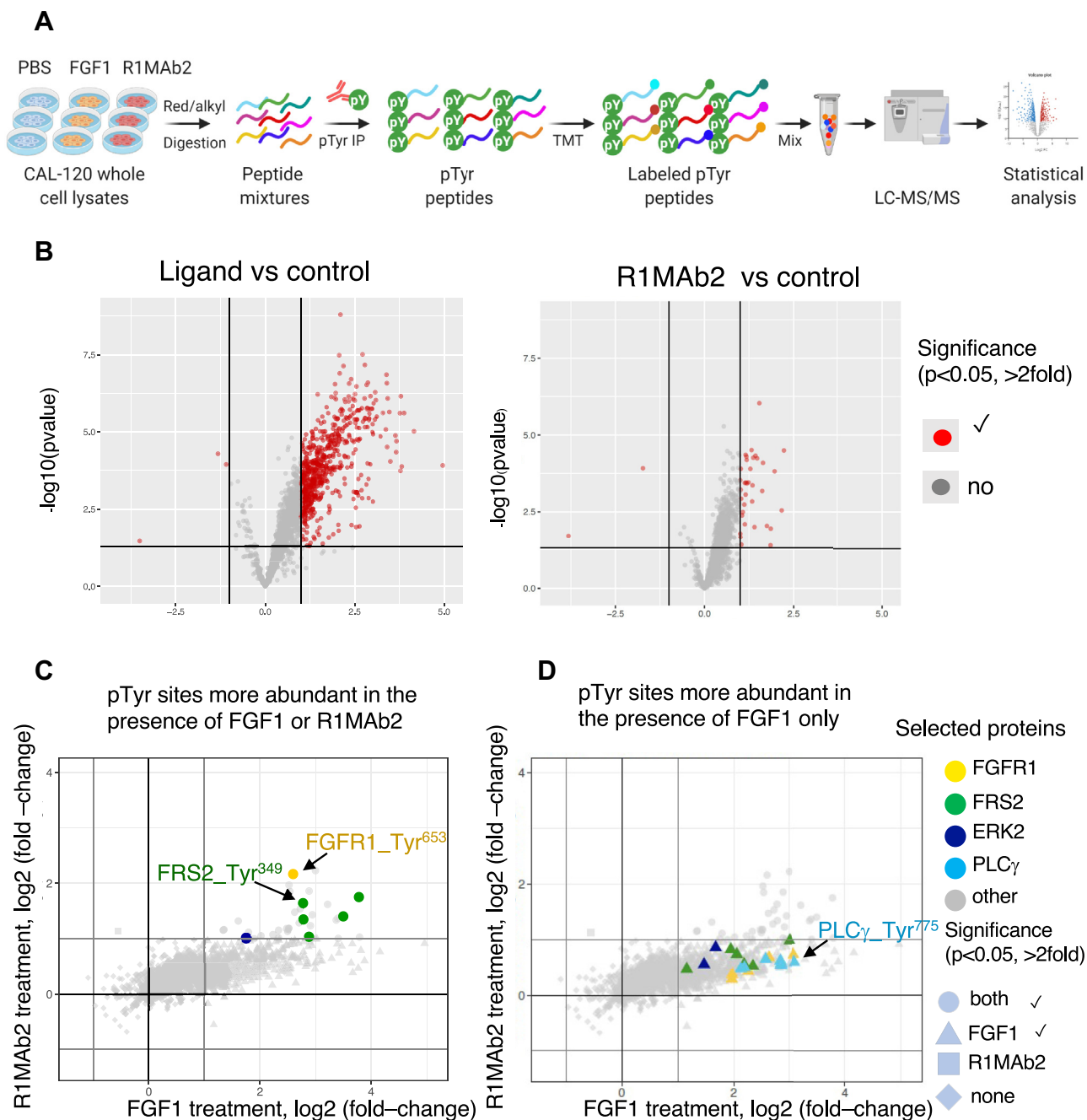


Figure 5. Assessment of phospho-tyrosine profile differences in CAL-120 treated with R1Mab2 or FGF1. A, illustration of experimental workflow of phospho-tyrosine affinity enrichment. B, volcano plots representing the changes in peptide abundance between control and FGF1- (left) or R1Mab2-treated (right) samples. Peptides with significant (Linear mix-effects model: $p < 0.05$) changes greater than 2-fold are plotted in red. C and D, comparison of changes for pTyr sites abundance in FGF1-treated samples against R1Mab2-treated samples. Plots highlight sites more abundant upon (C) both treatments or (D) FGF1 treatment only. Colors reflect proteins of interest, and shape shows the significance of the change in abundance. FGFR1, Fibroblast growth factor receptor 1; pTyr, phospho-tyrosine.

proliferation either by preventing receptor dimerization, ligand binding, and/or stabilizing an auto-inhibited conformation of the receptor (38, 39). In addition, MAbs may elicit an antibody-dependent cell-mediated cytotoxicity or an antibody-dependent cellular phagocytosis response through Fc-mediated activity (32).

The conflicting reports of FGFR1 agonistic and antagonistic Abs leading to a similar phenotype *in vivo* prompted us to conduct a thorough investigation on the pharmacological

properties of a representative set of Abs (18, 26, 27, 40). Here, we showed that R1MAbs can function both as agonists and antagonists in a context-specific manner. R1Mab1 and R1Mab2 were obtained using phage display and selected for their agonistic FGF21-like antidiabetic, lipid-lowering, and weight loss properties in obese mice (18). However, dosing of these molecules in adult mice results in mild hypophosphatemia, which ultimately led to the discontinuation of these Abs as potential therapeutic candidates (19). Conversely,

Elucidation of the mode of action of FGFR1 monoclonal antibodies

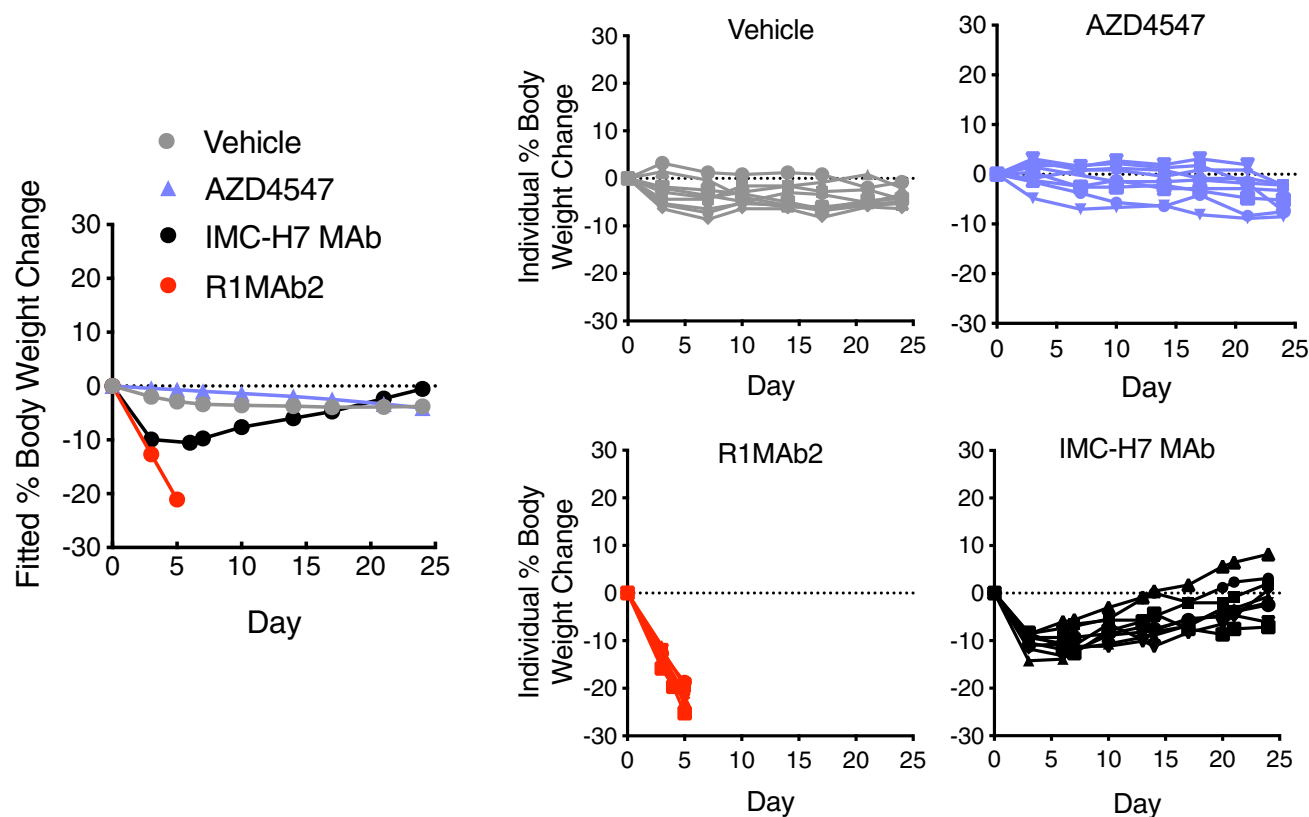


Figure 6. Impact of FGFR1 MABs and AZD4547 on weight loss in C.B-17 SCID mice inoculated with CAL-120 cells. Body weight changes of C.B-17 SCID mice bearing similar sized tumors after administration of vehicle, AZD4547, IMC-H7 MAb, or R1MAb2 were monitored. Grouped analysis and individual curves ($n = 9$ per group) are shown. FGFR1, Fibroblast growth factor receptor 1.

IMC-H7 MAB was selected for its antagonistic property suitable for anticancer therapy, but administration of IMC-H7 MAB unexpectedly led to weight loss in mice and monkeys through reversible hypophagia (26). Given the weight loss seen with IMC-H7 MAB treatment, we speculated that IMC-H7 MAB was not solely a FGFR1 antagonist as described. Indeed, we demonstrated that similar to R1MAbs, IMC-H7 MAB also displayed agonist behavior and induced significant proliferation of FGFR1-amplified CAL-120 cells. BLI-based epitope binning suggested that the epitopes of R1MAbs and IMC-H7 MAB partially overlapped on D2 but were distinct from the FGF-binding pocket. Therefore, we hypothesized that these MABs compete with FGF ligand binding through steric effects or a conformational change rather than a direct competition to exert their antagonist activity. However, in the absence of ligand, the bivalent IgGs acted as an FGFR1 agonist through the cross-linking of two FGFR1 monomers to drive cell proliferation.

Lelliott *et al.* characterize the dual agonist/antagonist activity of their FGFR1c MAB. While their FGFR1c MAB induces body weight loss in obese mice (27), the authors could not firmly conclude whether the physiological effect of their MAB could be attributed to the agonistic or antagonistic activity. Compelling evidence in the literature and clinical studies demonstrate the benefits of FGF21 mimetics for the treatment of metabolic disorders, suggesting that the activation of FGFR1c is responsible for the weight loss (17, 18, 41). In

addition, weight loss is not reported as an adverse effect for the FGFR small molecule inhibitors tested in the clinic for cancer indications (2). In our *in vivo* study, we compared side-by-side the FGFR1c MABs presenting a dual activity with a FGFR small molecule inhibitor and demonstrated that, in contrast to AZD4547, FGFR1c MABs treatment induced significant weight loss. Given the predominant agonistic effect of the MABs resulting in toxicity *in vivo*, we were unable to assess antagonistic effect of the MABs on tumor growth.

Depending on the desired therapeutic benefit (metabolic versus oncologic indications), one should carefully consider the activity of the MAB in both the presence and absence of ligand in order to identify molecules with the most optimal therapeutic index.

In addition to the dual antagonist/agonistic activity, our study highlighted a functionally distinct active FGFR1 conformation when bound to an mAb. In the presence of FGF, the ECDs of two adjacent FGFRs contact one another as well as heparin through the Ig-like domain D2 (IgD2) (12, 42). The epitopes of the FGFR1 MABs tested were located at the dimerization interface of IgD2. Consequently, the ECDs could not come into contact through D2 as they would in the FGFR1 active conformation. Consistent with the estimated distance between two FAb arms, the D2 domains were most likely about 6 to 12 nm apart (43). This hypothesis was supported by the lower TR-FRET signal measured between FGFR1 ECDs in the presence of MAB than the signal obtained with FGF2. The

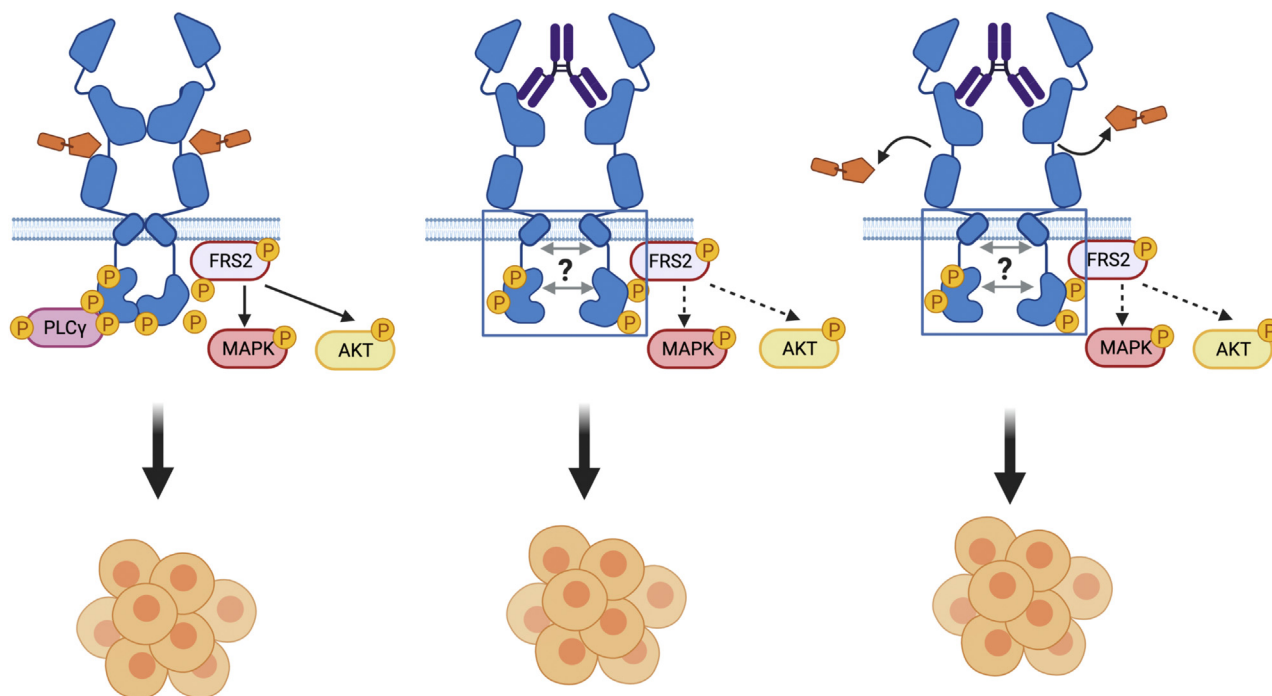


Figure 7. Proposed model of FGFR1 activation in the presence of FGF ligand, FGFR1 Ab alone (R1MAb or IMC-H7 MAb), or FGF ligand and FGFR1 MAb. In the presence of FGF, FGFR forms stable dimers with FGF contacting both receptors and both FGFR1 extracellular domains interacting through a small patch in D2. A conformational change occurs at the TM level that translates into full activation of the FRS2- and PLC γ -dependent signaling pathways. In the presence of the FGFR1 MAb, the ECDs are further apart and cannot interact through D2, which may result in a KD configuration favorable to phosphorylation events supporting FRS2-dependent signaling only and cell proliferation. When both MAb and FGF ligand are present, the MAb indirectly competes with FGF binding, and at high MAb concentration, a similar phenotype as previously described with MAb alone is observed. FGF, fibroblast growth factor; FGFR1, FGF receptor 1; KD, kinase domain.

MAb was therefore likely to stabilize a different orientation/conformation of the ECDs of adjacent FGFR1 monomers. How this translates into the relative conformation of the TM helices and the intracellular KDs remains to be elucidated. However, our signaling results supported a particular arrangement of both domains incompatible with full agonistic activity. Another possible explanation to the difference in signaling would be that FGF ligands and MAbs may differentially stabilize FGFR1 dimers similar to what was reported for EGFR ligands (44, 45).

Previous structure-function studies performed on EGFR fragments support the requirement for an N-terminal interaction between the TM helices to promote an antiparallel interaction between juxtamembrane segments, resulting in the formation of active asymmetric kinase dimerization. EGF binding acts by triggering this N-terminal interaction between the TM domains (46, 47). Similar observations are noted for FGFR, where a switch in the TM helices from unliganded FGFR dimers to ligand-specific configurations is reported in the presence of FGF1 and FGF2. FGF1- and FGF2-bound states are structurally and functionally distinct, with FGF2 resulting in the highest degree of phosphorylation (48). In the presence of R1MAb or IMC-H7 MAb, we hypothesized that the likelihood of obtaining such a fully functional TM helices switch was minimal due to the spacing of FGFR1 ECDs (~6–12 nm). Instead, the MAbs most likely stabilized an intermediate FGFR1 dimer state, in which the ECDs were loosely associated through antibody cross-linking, but the TM helices

position toward one another was suboptimal. Huang *et al.* describe the requirement for FGFR KDs to act in concert to recruit and transphosphorylate PLC γ (31). Our studies suggested an incorrect or suboptimal orientation of the KDs in the presence of the tested MAbs. Under this configuration, only residue pTyr⁶⁵³ on FGFR1 was phosphorylated, suggesting that the accessibility to other potential phosphorylation sites may have been a limiting factor. We did not see any additional unexpected phosphorylation of tyrosine. Of note, we did not assess phosphorylation of serine threonine sites. It should be noted that FGFR1 phosphorylation sites are phosphorylated with different kinetics, pTyr⁶⁵³ being among the first sites to be activated and Tyr⁷⁶⁶ the latest. It is thus reasonable to hypothesize that the biased agonism observed toward the FRS2-mediated pathway is the result of a partial activation signal that is insufficient to reach a threshold and trigger the phosphorylation events further downstream.

In contrast to PLC γ , the adaptor molecule FRS2 is constitutively bound to the FGFR1 juxtamembrane region. The unique phosphorylation of pTyr⁶⁵³ on FGFR1 was sufficient to induce phosphorylation of most of the pTyr sites on FRS2. Both R1MAb and IMC-H7 MAb increased CAL-120 proliferation, which was in line with the activation of the FRS2-dependent MAPK signaling pathway (8), and further supported that PLC γ recruitment was not required to induce cell proliferation.

Our work has implications for the design of agonistic or antagonistic MAbs targeting FGFR or other RTK molecules.

Elucidation of the mode of action of FGFR1 monoclonal antibodies

For example, our FAb data provided additional support for the strategy of developing monovalent one-armed Abs as RTK antagonists (49). For a FGFR agonist, designing molecules that target different epitopes and/or possess various geometries will be required to maximize pathway activation. For example, several reports observe diverse signaling profiles for RTK and cytokine receptors in the presence of mAbs or other engineered molecules capable of inducing ECD dimerization (50–53). In some cases, dimerization alone does not suffice to trigger a full agonistic response (52). In addition to proximity, the receptor geometry matters. Garcia *et al.* conducted a thorough investigation to determine the relationship between receptor topography and modulation of signaling outputs (54, 55). By designing a series of surrogate DARPin ligands to systematically alter the angle and distance between erythropoietin receptor, they were able to generate a range of full, biased, and partial agonism of erythropoietin receptor signaling (54, 55). Translating these results to the FGFR and RTK field will be important to designing agonistic molecules for metabolic indications.

Overall, our study provided insight into the challenges of developing antibody therapeutic molecules, especially toward dimeric cell-surface receptors. It highlighted the importance of optimizing several functional assays in the presence or absence of the endogenous ligand for lead selection so that both agonist and antagonist activities can be properly assessed. In addition, it is necessary to ensure that these assays can capture signaling events occurring along the entire signaling pathway in order to identify agonists that may display a functional behavior different from the natural ligands and induce the desired effect *in vivo*. Our study supported the possibility to modulate signaling outputs by stabilizing specific receptor conformations and has implications for the development of therapeutic Abs toward dimeric receptors beyond the FGFR field.

Experimental procedures

Generation of Abs and FGFR1c-Fc

Constructs for mammalian expression of IgGs and FAbs for R1MAb1, R1MAb2, and IMC-H7 were generated in house by gene synthesis. Plasmids encoding for the light chain and heavy chain were cotransfected into HEK293 cells and purified using a HiTrap column (GE Healthcare) with MabSelect Sure resin (GE Healthcare) followed by size-exclusion chromatography (SEC) with a Superdex S200 10/300 G1 size exclusion column (GE Healthcare) (56). To generate protein for epitope binning, a construct encoding Asn¹⁴³-Ser³⁷¹ of FGFR1b followed by a C-terminal His tag was used. The plasmid was transfected into HEK293 cells and purified using Ni-NTA Superflow resin (Qiagen) followed by SEC with a Superdex S200 10/300 G1 size exclusion column (GE Healthcare). To generate the FGFR1c receptor as a ligand trap, a construct encoding Met¹-Lys³⁶³ of FGFR1c followed by the sequence of human IgG1 Fc (EU numbering, Asp²²¹-Lys⁴⁴⁷) was used. The plasmid was transfected into HEK293 cells and purified using a HiTrap column (GE Healthcare) with MabSelect Sure resin

(GE Healthcare) followed by SEC with a Superdex S200 10/300 G1 size exclusion column (GE Healthcare).

Epitope binning using Octet

Epitope binning of the Abs was completed using cross competition assays performed on an Octet Red-384 system (ForteBio/Sartorius) using BLI. The cross-competition assays employed a classic sandwich strategy. Anti-human Fc capture biosensors were used to capture human IgG1 constructs of each Ab using a concentration of 25 µg/ml in blocking buffer (PBS, 0.5% bovine serum albumin (BSA), 15 PPM Proclin; Sigma Aldrich) at 25 °C for 300 s (“Capture#1”). The captured Abs were then incubated with His-tagged FGFR1b protein (N143-S371) at 25 µg/ml in blocking buffer at 25 °C for 200 s to allow binding and complex formation between the captured Abs and target protein (“Capture#2”). The biosensors containing the Ab-antigen complexes were finally incubated with various FAbs at 25 µg/ml in blocking buffer at 25 °C for 300 s (“Capture#3”). An increase in signal (nm) recorded by the biosensors indicates that the FAb can simultaneously bind to FGFR1 in the presence of the IgG and that these two Abs occupy nonoverlapping epitopes. No increase in signal (nm) recorded by the biosensors indicates that the FAb cannot simultaneously bind to FGFR1 in the presence of the IgG and that these two Abs occupy overlapping epitopes.

Cell culture

Engineered U2OS cells expressing ProLink (PK)-tagged FGFR1 and an enzyme acceptor-tagged PLCγ1 were purchased from DiscoverX and cultured according to the manufacturer's instructions. All other cell lines were from the Genentech cell line repository and were tested for *Mycoplasma*. CAL120 cells were maintained in Roswell Park Memorial Institute (RPMI) 1640 medium supplemented with 10% fetal bovine serum (FBS) and 2 mM L-Glutamine. COS7 were cultured in Dulbecco's modified Eagle's medium supplemented with 10% FBS and 2 mM L-Glutamine. MDA-MB-134-VI were cultured in Leibovitz's L15 media supplemented with 20% FBS and 2 mM L-Glutamine.

FGFR1 MABs cell-binding competition assay

COS7 cells expressing human FGFR1c were seeded in cold binding buffer (Opti-minimal essential medium + 2% FBS + 50 mM 4-(2-hydroxyethyl)-1-piperazineethanesulfonic acid [Hepes], pH 7.2 + 0.1% Sodium Azide) at 100,000 cells per well. A fixed concentration of Iodine-125 FGF2 (R&D Systems, #233-FB-500/CF/lot HKW14318113) radiolabeled using the NEX244 Iodogen method (PerkinElmer) was mixed with serially diluted FGFR1 MABs starting at 333 nM. The antibody mixture was added to the cells and incubated at room temperature for 2 h under gentle agitation. The cells and Abs were then transferred to Millipore multiscreen filter plates. The filter plates were washed 4 times with 250 µl of cold binding buffer and dried for at least 30 min, and the filters were punched into 5 ml polystyrene tubes. The radioactivity was measured using a PerkinElmer Wallac Wizard 2470 Gamma

Elucidation of the mode of action of FGFR1 monoclonal antibodies

Counter set at 1 count per minute with 0.8 counting efficiency. The data were fitted using the heterologous one site-fit Ki competitive binding model in GraphPad Prism.

MSD Phospho-FRS2 (Tyr196) assay

COS7 cells were transiently transfected with vectors encoding receptor FGFR1 using Lipofectamine 2000 according to the manufacturer's instructions (Life Technologies, Inc.) and seeded at 100,000 cells/well in a 96-well plate. After a 24-h incubation at 37 °C, 5% CO₂, transfected cells were cultured for 2 h in serum-free medium with FGF2 ligand and/or FGFR1 Abs at various concentrations. Cells were then lysed using complete lysis buffer provided in the MSD Phospho-FRS2 (Tyr196) Assay Whole Cell Lysate Kit (K150KJD-2). Phospho-FRS2 was measured using the MSD multiassay assay system per the manufacturer's instructions (MSD).

GAL-ELK1 luciferase reporter assay

COS7 cells were transiently transfected with vectors encoding receptor FGFR1c, a transcriptional activator (pFA2-Elk1), a firefly luciferase reporter gene driven by GAL4-binding sites (pFR-luc), and a Renilla luciferase (RLSV40) using Lipofectamine 2000 according to the manufacturer's instructions (Life Technologies, Inc.). Cells were seeded (100,000 cells/well) in a 96-well plate and incubated overnight. On the next day, transfected cells were cultured for an additional 6 h in serum-free medium with FGF ligand and/or IgG protein at various concentrations. The luciferase activity was determined using Dual-Glo Luciferase Assay System (Promega) and a CLARIOstar reader (BMG LABTECH).

PLCγ1 recruitment assay

Engineered U2OS cells expressing ProLink (PK)-tagged FGFR1 and an enzyme acceptor-tagged PLCγ1 (DiscoverX) were plated (40,000 cells/well) in a 384-well plate and incubated overnight at 37 °C, 5% CO₂. After a 24 h incubation, cells were cultured with FGF ligand and/or FGFR1 Abs diluted in DiscoverX-recommended medium for 22 h. Following stimulation, signal was detected using the PathHunter Detection Kit according to the recommended protocol. The signal was recorded with a CLARIOstar reader (BMG LABTECH).

Western blot

CAL-120 or MDA-MB-134-VI cells were serum-starved in 0.1% BSA RPMI 1640 medium for 4 h. Cells were then treated with either 15 ng/ml FGF1 (R&D Systems, #232-FA/lot CQ3518101) and 10 µg/ml heparin (Sigma) for 30 min or 1 µg/ml R1MAb2 for 1 h. To prepare extracts for immunoblotting, cells were washed once with ice-cold PBS and lysed with Cell Extraction Buffer (Invitrogen) containing protease (Roche) and phosphatase inhibitors (Sigma). Insoluble material was removed by centrifugation, and protein concentration was determined using a BCA Protein Assay (Pierce). Equal amounts of protein lysates were loaded onto a 4 to 12% NuPage Bis-Tris gel (Invitrogen). Proteins were transferred using the iBlot Gel Transfer Device (Invitrogen). Rabbit Abs to

phospho-PLCγ1 (Tyr⁷⁸³) (#14008/lot 4), PLCγ1 (#5690/lot 1), phospho-CREB (Ser¹³³) (#9198/lot 18), CREB (#9197/lot 17), phospho-FRS2 (Tyr¹⁹⁶) (#3864/lot 5), phospho-FRS2 (Tyr⁴³⁶) (#3861/lot 5), phospho-FGFR (Tyr^{653/654}) (#52928/lot 1), phospho-FGFR1 (Tyr⁷⁶⁶) (#84309, lot 1), FGFR1 (#9740/lot 4), phospho-ERK (Thr²⁰²/Tyr²⁰⁴) (#9101/lot 30), ERK1/2 (#9102/lot 27), phospho-AKT (Ser⁴⁷³) (#4060/lot 24), and AKT (#9272/lot 27) were obtained from Cell Signaling, FRS2 (#ab183492/lot GR153352-9) from Abcam, mouse Abs to GAPDH (#MAB374/lot 2955484) from EMD Millipore and to β-actin (#A5441/lot 127M48667) from Sigma. Specific antigen-antibody interaction was detected with a horseradish peroxidase-conjugated secondary goat anti-rabbit IgG (Jackson ImmunoResearch, #111-035-144/lot 132409) or goat anti-mouse IgG (Jackson ImmunoResearch, #115-035-146/lot 139407) using enhanced chemiluminescent detection reagents SuperSignal West Pico or Femto Chemiluminescent Substrates (Pierce). Films were scanned on an Epson Perfection V600 Photo scanner and images were quantified using ImageJ (National Institutes of Health).

Cell proliferation assay

CAL-120 cells were plated in growth medium containing 1% FBS and heparin (10 µg/ml) in the presence or absence of FGF1 at 1000 cells/well in 96-well ultra-low attachment plates (Costar) after passing through a 70 µm cell strainer (Falcon). The following day, treatments were serially diluted starting at the indicated concentrations, then added to cells in triplicate. AZD4547 was obtained from Selleckchem as a 10 mM dimethylsulfoxide stock solution. Seven days posttreatment, Promega's CellTiter-Glo 3D Luminescent Cell Viability Assay reagent was added per manufacturer's protocol. Luminescence was read using a PerkinElmer EnVision Multilabel Plate Reader.

qRT-PCR assay

CAL-120 cells were plated in growth medium containing 1% FBS at 600,000 cells/well in 8-well plates. The next day, cells were treated as indicated. Eight hours posttreatment, total RNA was extracted using Ambion's MagMAX-96 Total RNA Isolation kit and the KingFisher Flex instrument. RNA expression was determined using predesigned TaqMan gene expression assays (DUSP4 Hs01027785_m1, DUSP6 Hs00169257_m1, FOSL1 Hs04187685_m1, SPRY4 Hs00540086_m1, GAPDH Hs02758991_g1) and TaqMan RNA-to-Ct 1-Step Kit using a ViiA 7 Real-Time PCR System (Applied Biosystems).

Intracellular calcium measurement

Black 384-well culture plates with clear bottoms were seeded with 20,000 CAL-120 cells/well and incubated overnight. Cells were then incubated with a dye loading solution including a calcium indicator dye (BD Biosciences), probenecid (BD Bioscience), and 1× enhancer (BD Bioscience) in Hank's balanced salt solution buffer (GIBCO) containing 0.02% BSA (R&D Systems) and 20 mM Hepes

Elucidation of the mode of action of FGFR1 monoclonal antibodies

adjusted to pH 7.4 for 1 h at 37 °C, 5% CO₂. FGF ligand and/or FGFR1 Abs were added at various concentrations, and the signal was recorded using an uFDSS instrument (Hamamatsu) with excitation of 485 nm and emission of 525 nm.

SNAP-tag labeling and TR-FRET measurement

Stable COS7 cells expressing N-terminus SNAP-tagged FGFR1 were seeded in a white 96-well plate and incubated overnight at 37 °C, 5% CO₂. Cells were then labeled with 100 nM donor-conjugated benzyl-guanine SNAP-Lumi4-Tb (PerkinElmer) and 1 μM acceptor-conjugated benzyl-guanine SNAP-A467 (New England BioLabs) diluted in Dulbecco's modified Eagle's medium containing 10% FBS for 1 h at 37 °C, 5% CO₂. After three washes in PBS, the Lumi4-Tb emission and the TR-FRET signal were recorded at 620 and 665 nm, respectively, at t = 0 and t = 15 min postligand addition using a CLARIOstar reader (BMG LABTECH). The TR-FRET intensity was calculated as followed: (signal at 665 nm from cells labeled with SNAP donor and SNAP acceptor) - (signal at 665 nm from the same population of transfected cells labeled with SNAP donor and non-labeled SNAP). The TR-FRET ratio represents the TR-FRET intensity divided by the donor emission at 620 nm.

Phospho-kinase arrays

CAL-120 cells were plated in growth medium at 3,000,000 cells per 10-cm plate. The following day, cells were serum-starved in 0.1% BSA RPMI 1640 for 4 h. Cells were then treated with either 15 ng/ml FGF1 and 10 μg/ml heparin for 30 min or 1 μg/ml R1MAb2 for 1 h. Cells were washed once with ice-cold PBS and lysed with Cell Extraction Buffer (Invitrogen) containing protease (Roche) and phosphatase inhibitors (Sigma). Insoluble material was removed by centrifugation, and protein concentration was determined by BCA Protein Assay (Pierce). Differences in phospho-protein levels were assessed using Proteome Profiler Human Phospho-Kinase Array Kit (R&D Systems) according to the manufacturer's protocol.

PLCγ1 and FGFR1 knockdowns

ON-TARGETplus Nontargeting Control Pool (D-001810-10-20), ON-TARGETplus Human *PLCG1* siRNA (L-003559-00-0005), and ON-TARGETplus Human *FGFR1* siRNA (L-003131--00-0020) were obtained from Dharmacon. For *PLCγ1* knockdown, RNAiMAX Transfection Reagent (Invitrogen) was used to deliver 50 nM siRNA to CAL-120 cells plated at 300,000 cells/well in 8-well plates. At 48 h post-transfection, cells were serum-starved in 0.1% BSA RPMI 1640 for 4 h. Cells were then treated with either 15 ng/ml FGF1 and 10 μg/ml heparin for 30 min or 1 μg/ml R1MAb2 for 1 h, and Western blot analysis was conducted as described in the [Experimental procedures](#) section above.

For *FGFR1* knockdown, CAL-120 cells were transfected using RNAiMAX Transfection Reagent (Invitrogen) with 10 nM siRNA and plated at 2500 cells per well in 96-well ultra-

low attachment plates (Costar). Forty eight hours post-transfection, a cell proliferation assay was conducted as described in the [Experimental procedures](#) section above.

Proteomic sample preparation

CAL-120 cells were harvested and lysed in 20 mM Hepes at pH 8.0, containing 9 M urea, 1 mM sodium orthovanadate, 2.5 mM sodium pyrophosphate, and 1 mM β-glycerophosphate. Whole cell lysates from PBS-treated, FGF1-treated (20 min), and R1MAb2-treated (1 h) CAL-120 cells (3 bioreplicates per condition, total of nine samples) were digested with trypsin and prepared for proteomic analysis. Samples were sonicated using a Misonix Microson XL sonicator followed by centrifugation at 20,000g for 20 min at 15 °C. Protein concentration was determined using a Bradford assay (Bio-Rad). Samples were reduced in 5 mM DTT at 37 °C for 1 h followed by alkylation with 15 mM iodoacetamide at room temperature for 20 min in the dark. Proteins were subjected to a serial digestion using Lys-C (Wako) at an enzyme:substrate (E:S) ratio of 1:50 at 37 °C for 4 h followed by tryptic digestion (Promega) at an E:S ratio of 1:50 at 37 °C overnight in 2 M urea. The peptide mixture was acidified with 20% TFA and desalted using C₁₈ cartridge (500 mg absorbent) from Waters. Peptides were eluted with 3 × 2.0 ml of 60% acetonitrile (ACN)/0.1% TFA followed by peptide concentration measurement using a quantitative colorimetric peptide assay kit (Thermo Fisher Scientific). Equal amounts of peptides per condition (17 mg) were aliquoted and lyophilized overnight.

Immunoaffinity enrichment of pTyr peptides and tandem mass tag labeling

Immunoaffinity capture of pTyr peptides was performed using the antibody-recognizing pTyr motif according to the PTMScan protocol published by Rush *et al.* (57). PTMScan Proteomics System was in-licensed from Cell Signaling Technologies. The enriched peptide mixture was dried down completely followed by chemical labeling with tandem mass tag (TMT) (Thermo Fisher Scientific) for quantitation. The dried peptide mixture was reconstituted in 20 μl of Hepes (200 mM, pH 8.5) + 3 μl of ACN + 5 μl TMT reagent (each vial of 0.8 mg of TMT reagent was reconstituted in 40 μl of ACN). Labeling was performed at room temperature for 1.5 h. From each condition, 1 μl was mixed, desalted, and analyzed to determine labeling efficiency. The reaction was quenched with 5% hydroxylamine once labeling efficiency was determined to be at least 95%. Samples were mixed at equal amounts followed by desalting and drying. The dried peptides from the 9-plex were subjected to a second round of immunoaffinity enrichment to minimize nonspecificity. The resulting enriched peptide mixture was desalted and dried prior to mass spectrometry analysis. TMT channels were assigned as followed: PBS, replicate 1, TMT10-126, 126.1277; PBS, replicate 2, TMT10-127N, 127.1246; PBS, replicate 3, TMT10-127C, 127.1309; FGF1-treated, replicate 1, TMT10-128N, 128.1281; FGF1-treated, replicate 2, TMT10-128C, 128.1341; FGF1-treated, replicate 3, TMT10-129N, 129.1317; R1MAb2-

treated replicate 1, TMT10-129C, 129.1376; R1Mab2-treated replicate 2, TMT10-130N, 130.1348, and R1Mab2-treated replicate 3, TMT10-130C, 130.1409.

Mass spectrometry analysis

The enriched pTyr peptides were reconstituted in 2% ACN/0.1% formic acid/water and loaded onto C₁₈ column (1.7 μm Ethylene Bridged Hybrid (BEH), 130 Å, 0.1 × 250 mm) (New Objective) using a NanoAcquity ultra performance liquid chromatography system (Waters) at a flow rate of 0.6 μl/min. A gradient of 2% to 30% solvent B (0.1% FA/2% water/ACN) at 0.5 μl/min was applied over 155 min with a total analysis time of 180 min to separate the peptides. Duplicate injections were made for technical replicates. Peptides were analyzed using an Orbitrap Lumos instrument (Thermo Fisher Scientific). Precursor ions (MS1) were analyzed in the Orbitrap (automatic gain control [AGC] target 1,000,000; 120,000 mass resolution, 50 ms maximum injection time), and the 10 most abundant species were selected for fragmentation (MS2). Ions were filtered based on charge state ≥ 2 ($z = 2, 3, \& 4-6$) and monoisotopic peak assignment, and dynamic exclusion (45 s ± 10 parts per million [ppm]) was enabled. Each precursor ion was isolated at a mass width of 0.5 Th followed by fragmentation using collision-induced dissociation (CID at 35 normalized collision energy); MS2 AGC target was set at 20,000 with a maximum injection time of 200 ms. Multiple fragment ions were isolated using synchronous precursor selection prior to higher energy collisional dissociation (55 normalized collision energy, synchronous precursor selection notches = 8, AGC target = 200,000, maximum injection time of 350 ms) MS3 fragmentation and Orbitrap analysis at 50,000 resolution.

Bioinformatics

Tandem mass spectrometry (MS/MS) data was searched using the Mascot search algorithm (Matrix Sciences) against a concatenated forward-reverse target-decoy database (UniProtKBconcat 2016_06) consisting of human proteins and common contaminant sequences. Spectra were assigned using a precursor mass tolerance of 50 ppm and fragment ion tolerance of 0.8 Da. Static modifications included carbamidomethyl cysteine (+57.0215 Da) and TMT (229.1629 Da) on both the N-terminus of the peptides and lysine residues. Variable modification included oxidized methionine (+15.994 Da) and phosphorylation on serine, threonine, and tyrosine residues (+79.9663 Da). Trypsin specificity with up to three miscleavages was specified. PSMs were filtered at 5% false discovery rate followed by protein filtering at 2% false discovery rate. A Score algorithm was used for phosphorylation site localization (58). For each PSM, TMT reporter ions were quantified with an in-house software package known as Mojave by calculating the highest peak within 20 ppm of theoretical reporter mass windows at MS3 level and correcting for isotope purities. Isolation specificity was calculated by dividing summed peak intensities from peptide precursor by total peak intensities within an isolation

window. A subset of pTyr peptides was filtered for further statistical analysis.

Statistical analysis of mass spectrometry data

Quantification and statistical testing of the TMT proteomics data was performed with MSstatsTMT v1.2.7, an open-source R/Bioconductor package. Prior to MSstatsTMT analysis, the PSMs were filtered as follows. PSMs were filtered out if they: (1) were from decoy proteins, (2) were from peptides with length less than 7 amino acids, (3) had an isolation specificity less than 0.5, and (4) had a summed reporter ion intensity (across all 9 channels) lower than 30,000. In the case of redundant PSMs (multiple PSMs in one MS run that map to the same peptide), the PSMs were summarized by summing the reporter ion intensities per peptide and channel. Next, MSstatsTMT summarized the peptide quantitation to the unique phosphorylation site level using Tukey median polish summarization. As a final step, the differential abundance analysis between conditions was performed in MSstats TMT based on a linear mixed-effects model per site. The inference procedure was adjusted by applying an empirical Bayes shrinkage.

Tumor xenograft study

In vivo studies were approved by Genentech's Institutional Animal Care and Use Committee (IACUC) and adhered to the ILAR Guide for the Care and Use of Laboratory Animals. Naïve, 14 to 15-week-old C.B-17 SCID.bg mice (Charles River Labs) were inoculated in the #2/3 mammary fat pad with 10 million CAL-120 cells suspended in Hank's balanced salt solution and matrigel (BD Biosciences). Once tumors reached a size of 127 to 217 mm³ ($x = 155.7 \pm 20.7$ mm³ SD), mice were randomized into treatment cohorts and test article administration began ($n = 9$ /group). The vehicle [0.5% methylcellulose, 1% Tween-80 (MCT)] and AZD4547 (12.5 mg/kg) groups were dosed orally, daily for 24 days. The IMC-H7 MAb and R1Mab2 groups, each received a single 1 mg/kg dose, intraperitoneally. Length (l) and width (w) of each tumor were measured using digital calipers (Fred V. Fowler Company, Inc.) and tumor volumes were calculated ($V = lw^2 \times 0.5$). Body weights were measured using an Adventurer Pro AV812 C scale (Ohaus Corporation).

Tumor growth analysis was performed using a package of customized functions in R (Version 4.1.0 [2021-05-18] R Foundation for Statistical Computing) (59). Estimates of group-level efficacy were obtained by calculating a growth contrast that represents the ratio of exponential tumor growth for the treatment and reference groups over a common study period. Exponential growth in each group is calculated by computing the area under the curve of the fit on the natural log scale for this time range, correcting the area under the curve for the starting tumor burden. Contrast values <1 indicate an antitumor effect; the smaller the value below 1, the greater the magnitude of the antitumor effect. A value of 1 is indicative of no treatment effect (*i.e.*, the daily fold changes are equivalent in both groups). Values in parenthesis indicate the

Elucidation of the mode of action of FGFR1 monoclonal antibodies

upper and lower boundaries of the 95% confidence interval for the difference based on the fitted model and variability measures of the data.

Data availability

All data are available in the main text or the supporting information.

Supporting information—This article contains supporting information.

Acknowledgments—We thank Hong Li and Ryan Abraham for protein reagents. We are grateful to Avi Ashkenazi for helpful discussions and to Stephen Gould for providing support for *in vivo* data representation and interpretation. Illustrations were created using BioRender. This study was funded by Genentech, Inc.

Author contributions—Jocelyn C., Joyce C., L. S., S. S. S., V. C. P., R. W. A., L. C., K. Y., and L. C.-A. investigation; Jocelyn C., Joyce C., L. S., V. C. P., R. W. A., L. C., K. Y. methodology; Jocelyn C., Joyce C., L. S., V. C. P., R. W. A., M. H., L. C., K. Y., J. T. K., G. S., and L. C.-A. visualization; S. S. S., J. T. K. resources; V. C. P., M. H., and K. Y. formal analysis; J. T. K., G. S., and L. C.-A. validation; J. T. K., G. S., and L. C.-A. conceptualization; J. T. K., G. S., and L. C.-A. supervision; J. T. K. and G. S. writing—review and editing; G. S. project administration; L. C.-A. writing—original draft.

Conflict of interest—All authors were employees of Genentech, Inc. at the time of this study.

Abbreviations—The abbreviations used are: Abs, antibodies; ACN, acetonitrile; AGC, automatic gain control; BLI, bio-layer interferometry; BSA, bovine serum albumin; CREB, cAMP response element-binding protein; ECD, extracellular domain; EGFR, epidermal growth factor receptor; FGF, fibroblast growth factor; FGFR1, FGF receptor 1; GAL, galactosidase; HSPG, heparan sulfate proteoglycan; IgG, immunoglobulin G; KD, kinase domain; MAPK, mitogen-activated protein kinase; PSM, peptide spectrum match; pTyr, phospho-tyrosine; RPMI, Roswell Park Memorial Institute; RTK, receptor tyrosine kinase; SEC, size-exclusion chromatography; TMT, tandem mass tag; TR-FRET, time-resolved FRET.

References

1. Beenken, A., and Mohammadi, M. (2009) The FGF family: biology, pathophysiology and therapy. *Nat. Rev. Drug Discov.* **8**, 235–253
2. Katoh, M. (2016) Therapeutics targeting FGF signaling network in human diseases. *Trends Pharmacol. Sci.* **37**, 1081–1096
3. Itoh, N., and Ornitz, D. M. (2004) Evolution of the Fgf and Fgfr gene families. *Trends Genet.* **20**, 563–569
4. Mohammadi, M., Olsen, S. K., and Ibrahimi, O. A. (2005) Structural basis for fibroblast growth factor receptor activation. *Cytokine Growth Factor Rev.* **16**, 107–137
5. Plotnikov, A. N., Schlessinger, J., Hubbard, S. R., and Mohammadi, M. (1999) Structural basis for FGF receptor dimerization and activation. *Cell* **98**, 641–650
6. Wang, F., Kan, M., Yan, G., Xu, J., and McKeehan, W. L. (1995) Alternately spliced NH₂-terminal immunoglobulin-like Loop I in the ectodomain of the fibroblast growth factor (FGF) receptor 1 lowers affinity for both heparin and FGF-1. *J. Biol. Chem.* **270**, 10231–10235
7. Johnson, D. E., Lu, J., Chen, H., Werner, S., and Williams, L. T. (1991) The human fibroblast growth factor receptor genes: a common structural arrangement underlies the mechanisms for generating receptor forms that differ in their third immunoglobulin domain. *Mol. Cell Biol.* **11**, 4627–4634
8. Goetz, R., and Mohammadi, M. (2013) Exploring mechanisms of FGF signalling through the lens of structural biology. *Nat. Rev. Mol. Cell Biol.* **14**, 166–180
9. Kharitonov, A., Shiyanova, T. L., Koester, A., Ford, A. M., Micanovic, R., Galbreath, E. J., *et al.* (2005) FGF-21 as a novel metabolic regulator. *J. Clin. Invest.* **115**, 1627–1635
10. Razaque, M. S., and Lanske, B. (2007) The emerging role of the fibroblast growth factor-23-klotho axis in renal regulation of phosphate homeostasis. *J. Endocrinol.* **194**, 1–10
11. Tomlinson, E., Fu, L., John, L., Hultgren, B., Huang, X., Renz, M., *et al.* (2002) Transgenic mice expressing human fibroblast growth factor-19 display increased metabolic rate and decreased adiposity. *Endocrinology* **143**, 1741–1747
12. Schlessinger, J., Plotnikov, A. N., Ibrahimi, O. A., Eliseenkova, A. V., Yeh, B. K., Yayon, A., *et al.* (2000) Crystal structure of a ternary FGF-FGFR-heparin complex reveals a dual role for heparin in FGFR binding and dimerization. *Mol. Cell* **6**, 743–750
13. Chen, H., Xu, C. F., Ma, J., Eliseenkova, A. V., Li, W., Pollock, P. M., *et al.* (2008) A crystallographic snapshot of tyrosine trans-phosphorylation in action. *Proc. Natl. Acad. Sci. U. S. A.* **105**, 19660–19665
14. Furdulj, C. M., Lew, E. D., Schlessinger, J., and Anderson, K. S. (2006) Autophosphorylation of FGFR1 kinase is mediated by a sequential and precisely ordered reaction. *Mol. Cell* **21**, 711–717
15. Ornitz, D. M., and Itoh, N. (2015) The fibroblast growth factor signaling pathway. *Wiley Inter. Rev. Dev. Biol.* **4**, 215–266
16. Kliewer, S. A., and Mangelsdorf, D. J. (2019) A dozen years of discovery: insights into the physiology and pharmacology of FGF21. *Cell Metab.* **29**, 246–253
17. Sonoda, J., Chen, M. Z., and Baruch, A. (2017) FGF21-receptor agonists: an emerging therapeutic class for obesity-related diseases. *Horm. Mol. Biol. Clin. Invest.* **30**. <https://doi.org/10.1515/hmbci-2017-0002>
18. Wu, A. L., Kolumam, G., Stawicki, S., Chen, Y., Li, J., Zavala-Solorio, J., *et al.* (2011) Amelioration of type 2 diabetes by antibody-mediated activation of fibroblast growth factor receptor 1. *Sci. Transl. Med.* **3**, 113ra126
19. Wu, A. L., Feng, B., Chen, M. Z., Kolumam, G., Zavala-Solorio, J., Wyatt, S. K., *et al.* (2013) Antibody-mediated activation of FGFR1 induces FGF23 production and hypophosphatemia. *PLoS One* **8**, e57322
20. Courjal, F., Cuny, M., Simony-Lafontaine, J., Louason, G., Speiser, P., Zeillinger, R., *et al.* (1997) Mapping of DNA amplifications at 15 chromosomal localizations in 1875 breast tumors: definition of phenotypic groups. *Cancer Res.* **57**, 4360–4367
21. Katoh, M. (2019) Fibroblast growth factor receptors as treatment targets in clinical oncology. *Nat. Rev. Clin. Oncol.* **16**, 105–122
22. Gavine, P. R., Mooney, L., Kilgour, E., Thomas, A. P., Al-Kadhimi, K., Beck, S., *et al.* (2012) AZD4547: an orally bioavailable, potent, and selective inhibitor of the fibroblast growth factor receptor tyrosine kinase family. *Cancer Res.* **72**, 2045–2056
23. Chae, Y. K., Ranganath, K., Hammerman, P. S., Vaklavas, C., Mohindra, N., Kalyan, A., *et al.* (2017) Inhibition of the fibroblast growth factor receptor (FGFR) pathway: the current landscape and barriers to clinical application. *Oncotarget* **8**, 16052–16074
24. Qing, J., Du, X., Chen, Y., Chan, P., Li, H., Wu, P., *et al.* (2009) Antibody-based targeting of FGFR3 in bladder carcinoma and t(4;14)-positive multiple myeloma in mice. *J. Clin. Invest.* **119**, 1216–1229
25. Bai, A., Meetze, K., Vo, N. Y., Kollipara, S., Mazza, E. K., Winston, W. M., *et al.* (2010) GP369, an FGFR2-IIIb-specific antibody, exhibits potent antitumor activity against human cancers driven by activated FGFR2 signaling. *Cancer Res.* **70**, 7630–7639
26. Sun, H. D., Malabunga, M., Tonra, J. R., DiRenzo, R., Carrick, F. E., Zheng, H., *et al.* (2007) Monoclonal antibody antagonists of hypothalamic FGFR1 cause potent but reversible hypophagia and weight loss in rodents and monkeys. *Am. J. Physiol. Endocrinol. Metab.* **292**, E964–976
27. Lelliott, C. J., Ahnmark, A., Admyre, T., Ahlstedt, I., Irving, L., Keyes, F., *et al.* (2014) Monoclonal antibody targeting of fibroblast growth factor

- receptor 1c ameliorates obesity and glucose intolerance *via* central mechanisms. *PLoS One* **9**, e112109
28. Plotnikov, A. N., Hubbard, S. R., Schlessinger, J., and Mohammadi, M. (2000) Crystal structures of two FGF-FGFR complexes reveal the determinants of ligand-receptor specificity. *Cell* **101**, 413–424
 29. Harding, T. C., Long, L., Palencia, S., Zhang, H., Sadra, A., Hestir, K., *et al.* (2013) Blockade of nonhormonal fibroblast growth factors by FP-1039 inhibits growth of multiple types of cancer. *Sci. Transl. Med.* **5**, 178ra139
 30. Comps-Agrar, L., Dunshee, D. R., Eaton, D. L., and Sonoda, J. (2015) Unliganded fibroblast growth factor receptor 1 forms density-independent dimers. *J. Biol. Chem.* **290**, 24166–24177
 31. Huang, Z., Marsiglia, W. M., Basu Roy, U., Rahimi, N., Ilghari, D., Wang, H., *et al.* (2016) Two FGF receptor kinase molecules act in concert to recruit and transphosphorylate phospholipase Cgamma. *Mol. Cell* **61**, 98–110
 32. Sliwkowski, M. X., and Mellman, I. (2013) Antibody therapeutics in cancer. *Science* **341**, 1192–1198
 33. Baselga, J., Gelmon, K. A., Verma, S., Wardley, A., Conte, P., Miles, D., *et al.* (2010) Phase II trial of pertuzumab and trastuzumab in patients with human epidermal growth factor receptor 2-positive metastatic breast cancer that progressed during prior trastuzumab therapy. *J. Clin. Oncol.* **28**, 1138–1144
 34. Baselga, J., Smith, B. L., Rafferty, E. A., and Bombonati, A. (2012) Case records of the Massachusetts General Hospital. Case 16-2012. A 32-year-old woman with HER2-positive breast cancer. *N. Engl. J. Med.* **366**, 2018–2026
 35. Gianni, L., Pienkowski, T., Im, Y. H., Roman, L., Tseng, L. M., Liu, M. C., *et al.* (2012) Efficacy and safety of neoadjuvant pertuzumab and trastuzumab in women with locally advanced, inflammatory, or early HER2-positive breast cancer (NeoSphere): a randomised multicentre, open-label, phase 2 trial. *Lancet Oncol.* **13**, 25–32
 36. Garrett, C. R., and Eng, C. (2011) Cetuximab in the treatment of patients with colorectal cancer. *Expert Opin. Biol. Ther.* **11**, 937–949
 37. Yin, Y., Djakovic, S., Marsters, S., Tien, J., Peng, J., Tremayne, J., *et al.* (2015) Redesigning a monospecific anti-FGFR3 antibody to add selectivity for FGFR2 and expand antitumor activity. *Mol. Cancer Ther.* **14**, 2270–2278
 38. Schmitz, K. R., and Ferguson, K. M. (2009) Interaction of antibodies with ErbB receptor extracellular regions. *Exp. Cell Res.* **315**, 659–670
 39. Sliwkowski, M. X., Lofgren, J. A., Lewis, G. D., Hotaling, T. E., Fendly, B. M., and Fox, J. A. (1999) Nonclinical studies addressing the mechanism of action of trastuzumab (Herceptin). *Semin. Oncol.* **26**, 60–70
 40. Tsimafeyeu, I., Zaveleva, E., Stepanova, E., and Low, W. (2013) OM-RCA-01, a novel humanized monoclonal antibody targeting fibroblast growth factor receptor 1, in renal cell carcinoma model. *Invest. New Drugs* **31**, 1436–1443
 41. Kolumam, G., Chen, M. Z., Tong, R., Zavala-Solorio, J., Kates, L., van Bruggen, N., *et al.* (2015) Sustained brown fat stimulation and insulin sensitization by a humanized bispecific antibody agonist for fibroblast growth factor receptor 1/betaKlotho complex. *EBioMedicine* **2**, 730–743
 42. Lemmon, M. A., and Schlessinger, J. (2010) Cell signaling by receptor tyrosine kinases. *Cell* **141**, 1117–1134
 43. Saphire, E. O., Stanfield, R. L., Crispin, M. D., Parren, P. W., Rudd, P. M., Dwek, R. A., *et al.* (2002) Contrasting IgG structures reveal extreme asymmetry and flexibility. *J. Mol. Biol.* **319**, 9–18
 44. Freed, D. M., Bessman, N. J., Kiyatkin, A., Salazar-Cavazos, E., Byrne, P. O., Moore, J. O., *et al.* (2017) EGFR ligands differentially stabilize receptor dimers to specify signaling kinetics. *Cell* **171**, 683–695.e618
 45. Macdonald-Obermann, J. L., and Pike, L. J. (2014) Different epidermal growth factor (EGF) receptor ligands show distinct kinetics and biased or partial agonism for homodimer and heterodimer formation. *J. Biol. Chem.* **289**, 26178–26188
 46. Arkhipov, A., Shan, Y., Das, R., Endres, N. F., Eastwood, M. P., Wemmer, D. E., *et al.* (2013) Architecture and membrane interactions of the EGF receptor. *Cell* **152**, 557–569
 47. Endres, N. F., Das, R., Smith, A. W., Arkhipov, A., Kovacs, E., Huang, Y., *et al.* (2013) Conformational coupling across the plasma membrane in activation of the EGF receptor. *Cell* **152**, 543–556
 48. Sarabipour, S., and Hristova, K. (2016) Mechanism of FGF receptor dimerization and activation. *Nat. Commun.* **7**, 10262
 49. Merchant, M., Ma, X., Maun, H. R., Zheng, Z., Peng, J., Romero, M., *et al.* (2013) Monovalent antibody design and mechanism of action of onartuzumab, a MET antagonist with anti-tumor activity as a therapeutic agent. *Proc. Natl. Acad. Sci. U. S. A.* **110**, E2987–2996
 50. Li, W., Lan, H., Liu, H., Fu, Z., Yang, Y., Han, W., *et al.* (2013) The activation and differential signalling of the growth hormone receptor induced by pGH or anti-idiotypic monoclonal antibodies in primary rat hepatocytes. *Mol. Cell Endocrinol.* **376**, 51–59
 51. Nakano, K., Kojima, T., Kasutani, K., Senoh, C., Natori, O., Ishii, S., *et al.* (2009) Effective screening method of agonistic diabodies based on auto-crine growth. *J. Immunol. Met.* **347**, 31–35
 52. Muller-Newen, G., Kuster, A., Wijdenes, J., Schaper, F., and Heinrich, P. C. (2000) Studies on the interleukin-6-type cytokine signal transducer gp130 reveal a novel mechanism of receptor activation by monoclonal antibodies. *J. Biol. Chem.* **275**, 4579–4586
 53. Gonzalez-Magaldi, M., McCabe, J. M., Cartwright, H. N., Sun, N., and Leahy, D. J. (2020) Conserved roles for receptor tyrosine kinase extracellular regions in regulating receptor and pathway activity. *Biochem. J.* **477**, 4207–4220
 54. Mohan, K., Ueda, G., Kim, A. R., Jude, K. M., Fallas, J. A., Guo, Y., *et al.* (2019) Topological control of cytokine receptor signaling induces differential effects in hematopoiesis. *Science* **364**, eaav7532
 55. Moraga, I., Wernig, G., Wilmes, S., Gryshkova, V., Richter, C. P., Hong, W. J., *et al.* (2015) Tuning cytokine receptor signaling by re-orienting dimer geometry with surrogate ligands. *Cell* **160**, 1196–1208
 56. Maun, H. R., Jackman, J. K., Choy, D. F., Loyet, K. M., Staton, T. L., Jia, G., *et al.* (2019) An allosteric anti-tryptase antibody for the treatment of mast cell-mediated severe asthma. *Cell* **179**, 417–431.e419
 57. Rush, J., Moritz, A., Lee, K. A., Guo, A., Goss, V. L., Spek, E. J., *et al.* (2005) Immunoaffinity profiling of tyrosine phosphorylation in cancer cells. *Nat. Biotechnol.* **23**, 94–101
 58. Beausoleil, S. A., Villen, J., Gerber, S. A., Rush, J., and Gygi, S. P. (2006) A probability-based approach for high-throughput protein phosphorylation analysis and site localization. *Nat. Biotechnol.* **24**, 1285–1292
 59. Forrest, W. F., Alicke, B., Mayba, O., Osinska, M., Jakubczak, M., Piatkowski, P., *et al.* (2020) Generalized additive mixed modeling of longitudinal tumor growth reduces bias and improves decision making in translational oncology. *Cancer Res.* **80**, 5089–5097